Министерство науки и высшего образования Российской Федерации

ФЕДЕРАЛЬНОЕ ГОСУДАРСТВЕННОЕ АВТОНОМНОЕ ОБРАЗОВАТЕЛЬНОЕ УЧРЕЖДЕНИЕ ВЫСШЕГО ОБРАЗОВАНИЯ

“САНКТ-ПЕТЕРБУРГСКИЙ НАЦИОНАЛЬНЫЙ ИССЛЕДОВАТЕЛЬСКИЙ УНИВЕРСИТЕТ ИНФОРМАЦИОННЫХ ТЕХНОЛОГИЙ, МЕХАНИКИ И ОПТИКИ”

ВЫПУСКНАЯ КВАЛИФИКАЦИОННАЯ РАБОТА

МОДЫ ШЕПЧУЩЕЙ ГАЛЕРЕИ ЭЛЕКТРОНОВ В КВАНТОВОЙ ТОЧКЕ

Автор Рамезанпур Шахаб _____
(Фамилия, Имя, Отчество) (Подпись)

Направление подготовки (специальность) 12.04.03
(код, наименование)
Фотоника и оптоинформатика

Квалификация магистр
(бакалавр, магистр)

Руководитель ВКР Богданов А.А. к.ф.-м.н. _____
(Фамилия, И., О., ученое звание, степень) (Подпись)

К защите допустить

Руководитель ОП Белов П.А., д.ф.-м.н. _____
(Фамилия, И.О., ученое звание, степень) (Подпись)

“_____”_____ 20 ____г.

Санкт-Петербург, 2019 г.

Студент Рамезанпур Ш. Группа Z4240 Факультет ФТФ
(Фамилия, И. О.)

Направленность (профиль), специализация «Метаматериалы»

Консультант (ы):
а) _____ _____
(Фамилия, И., О., ученое звание, степень) (Подпись)

б) _____ _____
(Фамилия, И., О., ученое звание, степень) (Подпись)

ВКР принята “____”_____20 ____г.

Оригинальность ВКР __ _____%

ВКР выполнена с оценкой _____

Дата защиты “____”_____20 ____г.

Секретарь ГЭК _____ _____
(ФИО) (подпись)

Листов хранения _____

Демонстрационных материалов/Чертежей хранения _____

Ministry of Science and Higher Education

FEDERAL STATE AUTONOMOUS EDUCATIONAL INSTITUTION OF HIGHER PROFESSIONAL EDUCATION

"Saint Petersburg State University of Information Technologies, Mechanics and Optics"

GRADUATION THESIS

WHISPERING GALLERY MODES OF ELECTRONS IN QUANTUM DOT

Author Ramezanpour Shahab _____
(full name) (signature)

Subject area 12.04.03 Photonics and optoinformatics
(code, name of program track)

Degree level master
(Bachelor, Master)

Thesis supervisor Bogdanov A.A., PhD _____
(surname, initials, academic title, degree) (signature)

Approved for defense

Head of program Belov P.A., PhD, D.Sc _____
(surname, initials, academic title, degree) (signature)

"____" _____ 20 ____

St. Petersburg, 2019

Student Ramezanpour Sh. Group Z4240 Faculty PhE
(Surname, initials)

Subject area, program/major «Metatmaterials»

Consultant(s):
a) _____ _____
(surname, initials, academic title, degree) (signature)

b) _____ _____
(surname, initials, academic title, degree) (signature)

Thesis received "____"_____20 ____

Originality of thesis: _____%

Thesis completed with the grade: _____

Date of defense "____"_____20 ____

Secretary of State Exam Commission_____ _____
(ФИО) (подпись)

Number of pages _____

Number of supplementary materials/Blueprints _____

Introduction

Semiconductor Quantum Dot (QD) can be modeled as an artificial atom, and reveal discrete energy levels similar to an atom. It is shown in refs. [1-2] that by measuring current versus gate voltage, a QD has similar properties of atoms, as filling the shell structures in a 2D harmonic oscillator. It is discussed that electrons tend to fill the shell with parallel spin (ferromagnetic filling), according to the Hund's law. However, by applying a magnetic field, degenerate energy levels with plus/minus angular momentum would be split (Zeeman effect), which can change ground states of the QD. Besides, by introducing direct and exchange coulomb interaction, filling of the shells can be antiparallel (antiferromagnetic).

It is shown in ref. [3] that energy levels of InAs QD are as s-, p- and d-shell by using high-resolution capacitance spectroscopy and detecting maximums of the capacitance. Furthermore, it shows that applying magnetic field causes intermixing of p- and d-shells. In order to model interband spectroscopy, in ref. [4], Coulomb interaction between electrons and also electrons and holes are calculated and treated as a perturbation, where confining potential is considered parabolic and two-dimensional.

Quantum Dots can support states with high angular momentum. These states behave as Whispering Gallery Modes (WGMs) in optical resonator. The distribution of wavefunction associated to WGM is confined to the edges of QD, which can have applications in electronic lenses and resonators. It is shown in ref. [5] that WGM can be created in Graphene by an induction from scanning tunneling probe. The size of the circular trap can be tuned by the voltage of the back-gated Graphene device. It is shown in ref. [6] that WGM can be created in Oligothiophene nano-rings which can act as electronic resonator. It is shown in ref. [7] that WGMs can be used as a superpersistent currents in Dirac materials which has application in Qubits and Topological Insulators (TI) [8].

In a few electron QD, electrons can create a crystalization called Wigner Molecules (WM). In these dots, excited electrons can reveal different modes including WGM. Structural and optical properties of InP/GaInP QDs are studied in ref. [9], while in [10-11], it is shown that WGMs can be in the resonance of Wigner Molecules (WMs) ground state. Furthermore, zero-bias conductance anomalies (having conductance at zeo

bias voltage) in Quantum Point Contact (QPC) is explained by Wigner localization and alternating equilibrium and non-equilibrium of Kondo screening of different spin states [12-13].

Therefore, evaluating the energy spectra of the QD is challenging, since many parameters can affect it such as Coulomb interaction between the electrons, shape of the QD, magnetic field, etc. Furthermore, literature usually consider lateral QD with a zero thickness, however, our calculation reveals that even very small thickness of the QD can have significant effect on the energy spectra. Besides, due to the application of some of the modes in the QD such as lasing, lenses, electronic resonator, ..., we study WGMs in the lateral QD and its energy levels.

We evaluate the energy spectra of QD with both perturbation approach and variational method. Although, perturbation approach is simpler, it suits well for our structure, since we consider the QD which contains a few amount of electrons in the ground state and one or two electrons in the excited state. Although, the variational method is much more time-consuming, it takes into account the effect of the wavefunctions on each other. We could attain almost the same result from these two methods.

This thesis shows that the dimension of the QD including its height has a critical effect on the QD's energy spectra, therefore, it cannot be considered as a 2D harmonic oscillator. The Coulomb interaction is comparable to the energy of interband transition which cause intermixing energy bands even for zero magnetic field. It shows resonances along the height of the lateral dot which are quite unusual, and studies perturbation and topological effects on surface states in these dots and also in spherical and triangular ones.

1 OVERVIEW OF THE RESEARCH FIELD

1.1 Energy Spectra of a Few Electrons Lateral Quantum Dot

1.1.1 Shell Filling and Spin Effect

Reference [1] represents that adding an electron to a semiconductor quantum dot, "addition energy" is required which is similar to the real atom. However, this addition energy is greater than the interband energy, due to the coulomb interaction between the electrons. Vertical quantum dots are like a disk with a diameter around 10 times of its thickness. They can be modeled by two dimensional (2D) harmonic oscillators, since their lateral potential can be considered to have a cylindrical symmetry with soft walls. The artificial shells can be filled completely by the number of electrons 2, 6, 12, ..., which are considered as magic numbers. The addition energy is usually larger when the electron numbers are equal to the magic numbers. To study the magnetic field dependence, at a sufficiently small magnetic field (B< 0.4 T), spin filling obeys Hund's rule, while at higher magnetic fields (B> 0.4 T), the filling of states are with successive spin-up and spin-down.

Figure 1(a) shows the current at drain voltage $V = 150\,\mu V$ as a function of gate voltage V_g for a dot with diameter $D = 0.5\,\mu m$, where the picks are related to adding one electron to the dot. Figure 1(b) depicts the addition energy versus the electrons number N, for two different devices.

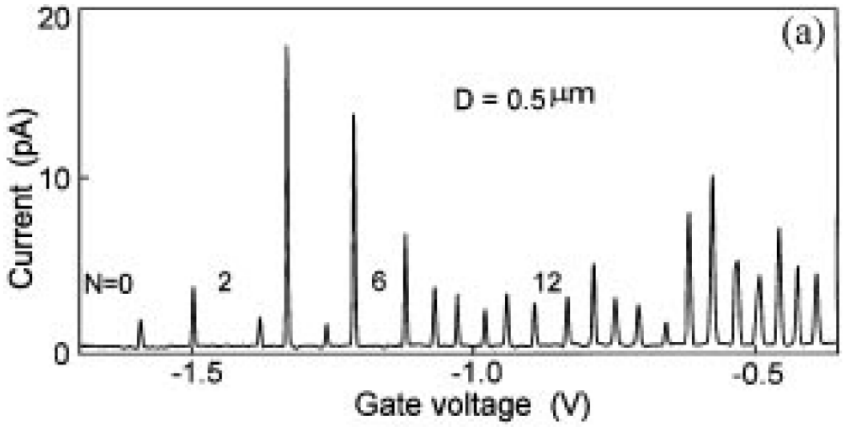

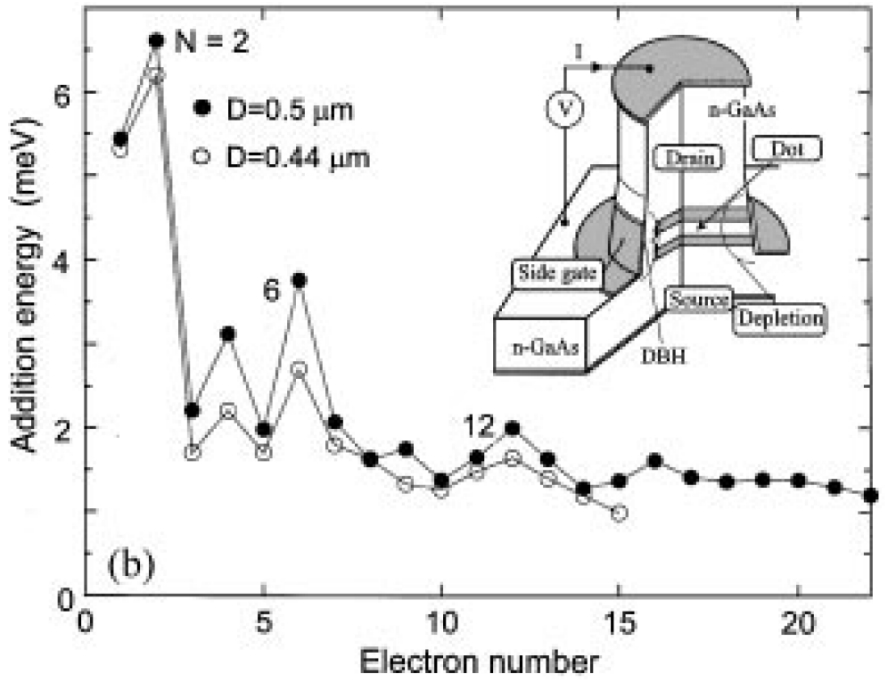

Figure 1 - (a) current versus gate voltage at $B = 0\,T$ for a $D = 0.5\,\mu m$ dot. (b) Addition energy versus electron number for two different dots with $D = 0.5\,\mu m$ and $0.44\,\mu m$ [1]

The energy spectrum in a *B* field for a 2D harmonic oscillator can be obtained analytically as:

$$E_{n,l} = (2n + |\ell| + 1)\hbar(\frac{1}{4}\omega_c^2 + \omega_0^2)^{1/2} - \frac{1}{2}\ell\hbar\omega_c$$

with a radial quantum number $n\,(= 0,1,2,...)$ and angular momentum quantum number $\ell\,(= 0, \pm 1, \pm 2, ...)$, while $\hbar\omega_0$ is the electrostatic confinement energy and $\hbar\omega_c$ is the cyclotron energy. Figure. 2(a) shows $E_{n,l}$ versus *B* calculated for $\hbar\omega_0 = 3meV$. A single-particle state with a positive angular momentum shifts lower while the state with a negative one shifts higher energies, respectively, with increasing *B*. Figure. 2(b) shows the *B*-field dependence of the fifth, sixth, and seventh current peaks. From this figure, one can observe that the fifth and sixth peaks form a pair. At 1.3 *T*, the maximum and minimum of the sixth and seventh peaks, respectively, can be attributed to the crossing of the third and fourth energy curves at 1.3 *T* in Fig. 2(a).

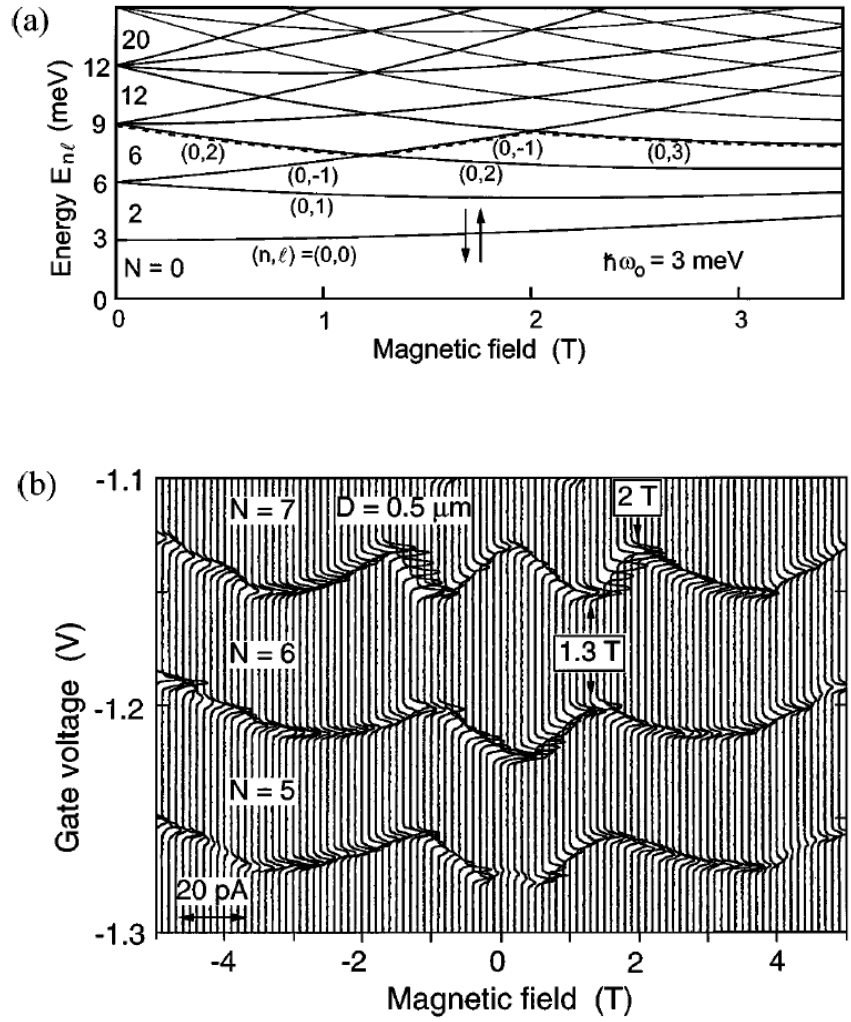

Figure 2 - (a) Calculated single-particle energy versus magnetic field for a parabolic potential with $\hbar\omega_0 = 3meV$. (b) Evolution of the fifth, sixth, and seventh current peaks with magnetic field for $D = 0.5\mu m$ dot [1]

1.1.2 Direct Coulomb and Exchange Interaction [2]

By applying magnetic field, ref. [2] shows that spin-configurations can be explained in terms of two-electron singlet and triplet states.

Figure. 3(b) shows two, spin-degenerate single-particle states with energies E_a and E_b crossing each other at $B = B_0$. For two electrons we can distinguish four possible configurations with either total spin $S = 0$ (spin-singlet) or $S = 1$ (spin-triplet). The corresponding energies, $U_i(2, S)$ for $i = 1$ to 4, are given by: $U_1(2, 0) = 2E_a + C_{aa}$ (two elctrons in E_a state with different spins),$U_2(2, 0) = 2E_b + C_{bb}$ (two electrons in E_b state with different spins), $U_3(2, 1) = E_a+E_b+C_{ab}-|K_{ab}|$ (one electron in E_a and another in E_b

state with same spin), $U_4(2, 0) = E_a + E_b + C_{ab}$ (one electron in E_a and another in E_b state with different spin), where C_{ij} and K_{ij} are direct and exchange Coulomb interaction, respectively.

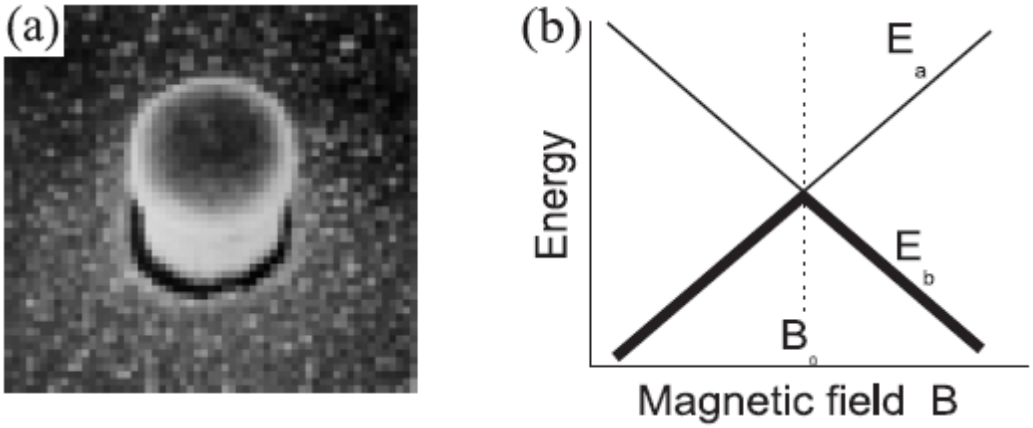

Figure 3 - (a) Scanning electron micrograph of the semiconductor quantum dot device. (b) Schematic diagram of two single particle states with energies E_a and E_b crossing each other at a magnetic field $B = B_0$ [2]

1.1.3 Capacitance-Voltage Traces of InAs Dot

Figure 4 shows the essential layer sequence and a sketch of the conduction band edge [3]:

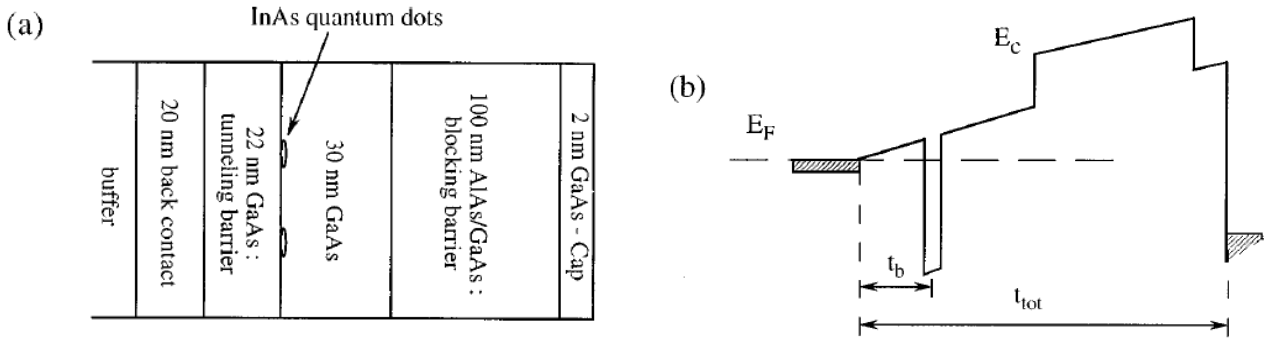

Figure 4 - (a) Layer sequence of the devices. The InAs dots are distributed within the plane sandwiched between two GaAs layers. (b) Sketch of the conduction-band edge E_c with respect to the Fermi level E_F along the growth direction for gate voltages at which no electrons are in the InAs dots. The indicated distances define the lever arm according to t_{tot}/t_b (in our case equal 7) which converts voltage into energy differences

Figure 5(a) shows the capacitance versus gate voltage for different applied magnetic fields between 0 and 23 *T*. It shows two degenerate maxima and four degenerate maxima, which can be attributed to the *s* and *p* shells, respectively. Figure 5(b) shows the dependence of these maximas to the magnetic field, which depicts that the maximas related to the s shell is almost unaffected (because of zero angular momentum), while two of the maximas related to the p shell decrease (because of positive angular momentum) and two of them increase (due to the negative angular momentum).

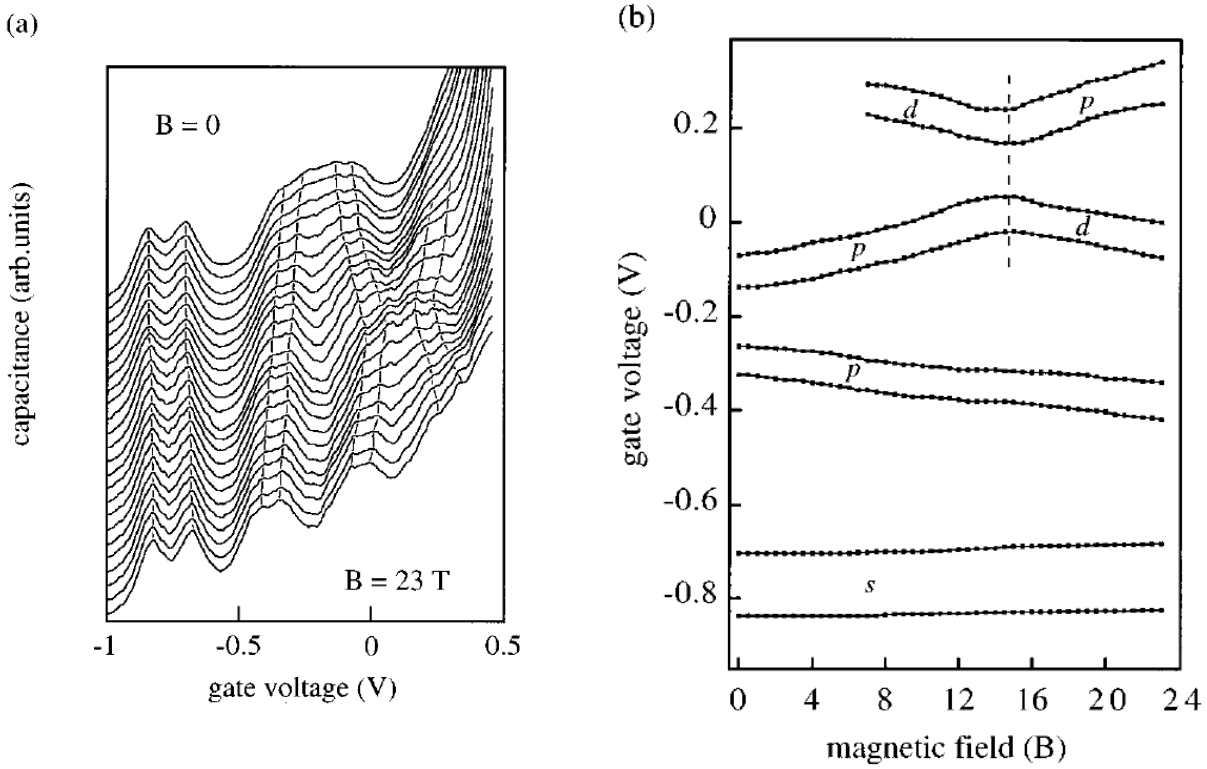

Figure 5 - (a) Differential capacitance of the layered structure at different magnetic fields (b) Magnetic-field dependence of each maxima [3]

1.1.4 Perturbation Approach for the Coulomb interactions between electrons

In magnetic field, single particle energies have the following energy levels:

$$\begin{aligned} & s, \quad \hbar\omega' \\ & p_- = 2\hbar\omega' - \frac{1}{2}\hbar\omega_c \\ & p_+ = 2\hbar\omega' + \frac{1}{2}\hbar\omega_c \\ & d_- = 3\hbar\omega' - \hbar\omega_c \\ & d_0 = 3\hbar\omega' \\ & d_+ = 3\hbar\omega' + \hbar\omega_c \end{aligned} \tag{1}$$

where

$$\omega' = \sqrt{\omega^2 + \omega_c^2 / 4} \tag{2}$$

is effective frequency and $\omega_c = eB/m^*$ is cyclotron frequency. For instance the s-state wavefunction is

$$\psi_s^e = \frac{1}{\sqrt{\pi} l_e} \exp(-r^2 / 2l_e^2) \tag{3}$$

where l_e is effective length of electrons

$$l_e = \sqrt{\frac{\hbar}{m^* \omega}} \tag{4}$$

while for holes effetive length is:

$$l_h = \sqrt{\frac{\hbar}{m_h^* \omega_h}} \tag{5}$$

On the other hand, direct and exchange Coulomb interaction can be obtained from Eqs. (6) and (7), respectively:

$$E_{ij} = \frac{e^2}{4\pi\varepsilon_0\varepsilon_r}\iint \frac{|\psi_i^e(\vec{r}_1)|^2 |\psi_j^e(\vec{r}_2)|^2}{|\vec{r}_1 - \vec{r}_2|} d\vec{r}_1 d\vec{r}_2 \tag{6}$$

$$E_{ij} = \frac{e^2}{4\pi\varepsilon_0\varepsilon_r}\iint \frac{\psi_i^e(\vec{r}_1)^* \psi_j^e(\vec{r}_2)^* \psi_i^e(\vec{r}_2)\psi_j^e(\vec{r}_1)}{|\vec{r}_1 - \vec{r}_2|} d\vec{r}_1 d\vec{r}_2 \tag{7}$$

For example, direct Coulomb interaction between two electrons in s-state is calculated:

$$E_{ij} = \frac{e^2}{4\pi\varepsilon_0\varepsilon_r}\sqrt{\frac{\pi}{2}}\frac{1}{l_e} \tag{8}$$

The ground state energy for N electrons can then be obtained from:

$$E_N = E^{sp}(N) + E^c(N) - \lambda^{-1} NeV_g \tag{9}$$

where $E^{sp}(N)$ is the sum of the single-particle energies, $E^C(N)$ the matrix element of the Coulomb interaction, and $-\lambda^{-1}NeVg$ expresses the electrostatic energy due to the electric field between gate and back contact.

1.2 Creating Whispering Gallery Modes

1.2.1 Graphene

In [5], Whispering Gallery Mode (WGM) is created in Graphene by creating pn junction, induced by a scanning tunneling probe (Fig. 6). The size of the resonator can be tuned by back-gated graphene device. It demonstrates an entirely different approach, inspired by the peculiar acoustic phenomena in whispering galleries. This type of resonators can be used in quantum electron-optics such as electronic lenses and resonators. Therefore, scanning tunneling microscopy (STM) probe is utilized for both probing electronic states and also creating pn junction which serves as confining potential for electrons.

Two types of WGM are detected in the structure (Fig. 7). First type is called WGM" which occur in conventional energy states $\varepsilon_\nu=\mu_0+eV_b$. However, the tip bias variation causes the Fermi level beneath the tip to move through system energy levels ε_ν, which create another type of WGM (WGM') at Fermi energy level $\varepsilon_\nu=\mu_0$.

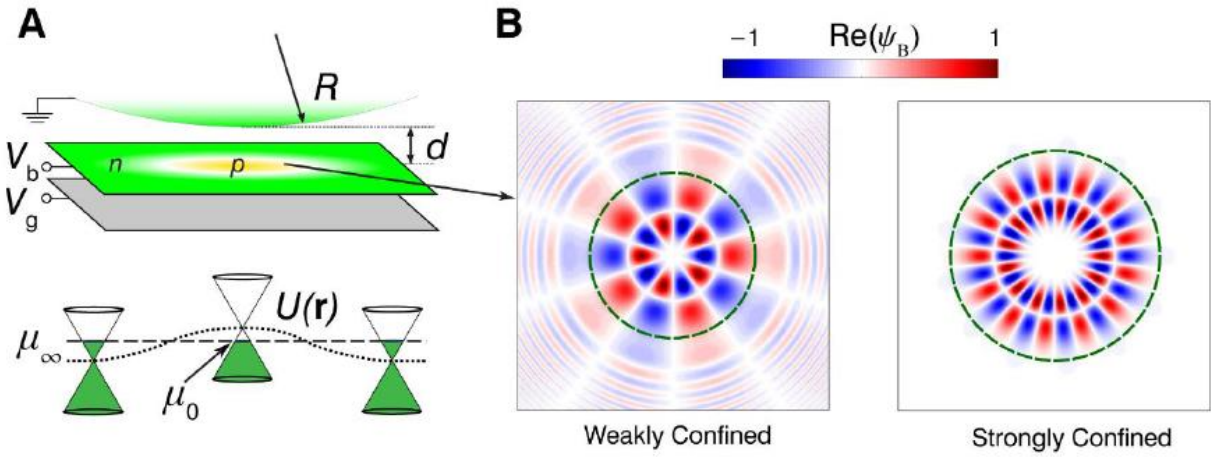

Figure 6 – (A) The rings are induced by the STM tip voltage bias (V_b) and back-gate voltage (V_g) is adjusted to reverse the carrier polarity beneath the tip relative to the ambient polarity. The cavity radius and the local carrier density are tunable by both V_b and V_g. (B) Spatial profile of WGM resonances. The confinement is stronger for the larger angular momentum *m* values [5]

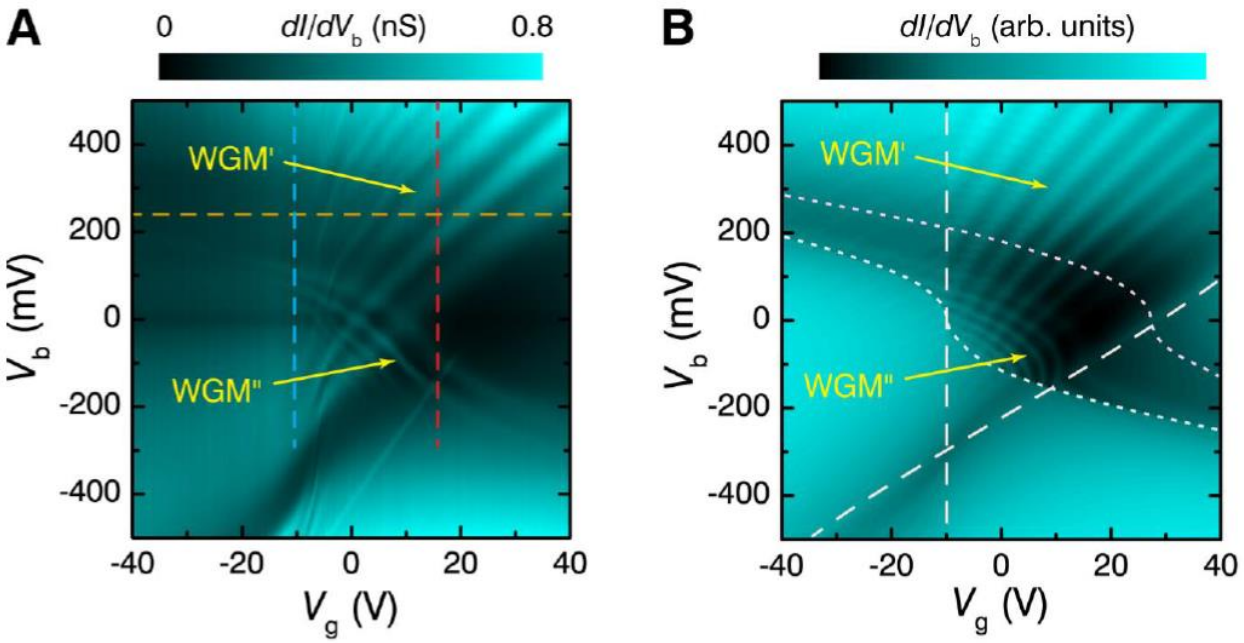

Figure 7 – (A) Differential tunneling conductance, dI/dV_b, map for a single-layer graphene device as a function of sample bias, V_b and back gate voltage, V_g. (B)

Interference features in dI/dV_b calculated from the relativistic Dirac model. The boundaries of WGM' (WGM") regions are marked by dashed (dotted) white lines [5]

1.2.2 Oligothiophene Nano-Rings

In Whispering gallery Modes (WGMs), such as the dome of St Paul's Cathedral in London, waves travel along a curved path. For closed-loop galleries, wave resonances appear when an integer number of wavelengths equals the perimeter of the resonator. To have WGM, the coherence length of the waves must exceed the perimeter of the resonator, and the walls must efficiently reflect the waves. Reference [6] creates WGM in Oligothiophene nano-rings as shown in Fig. 8. This figure also contains wire topology excitement, which has application in atomic wire.

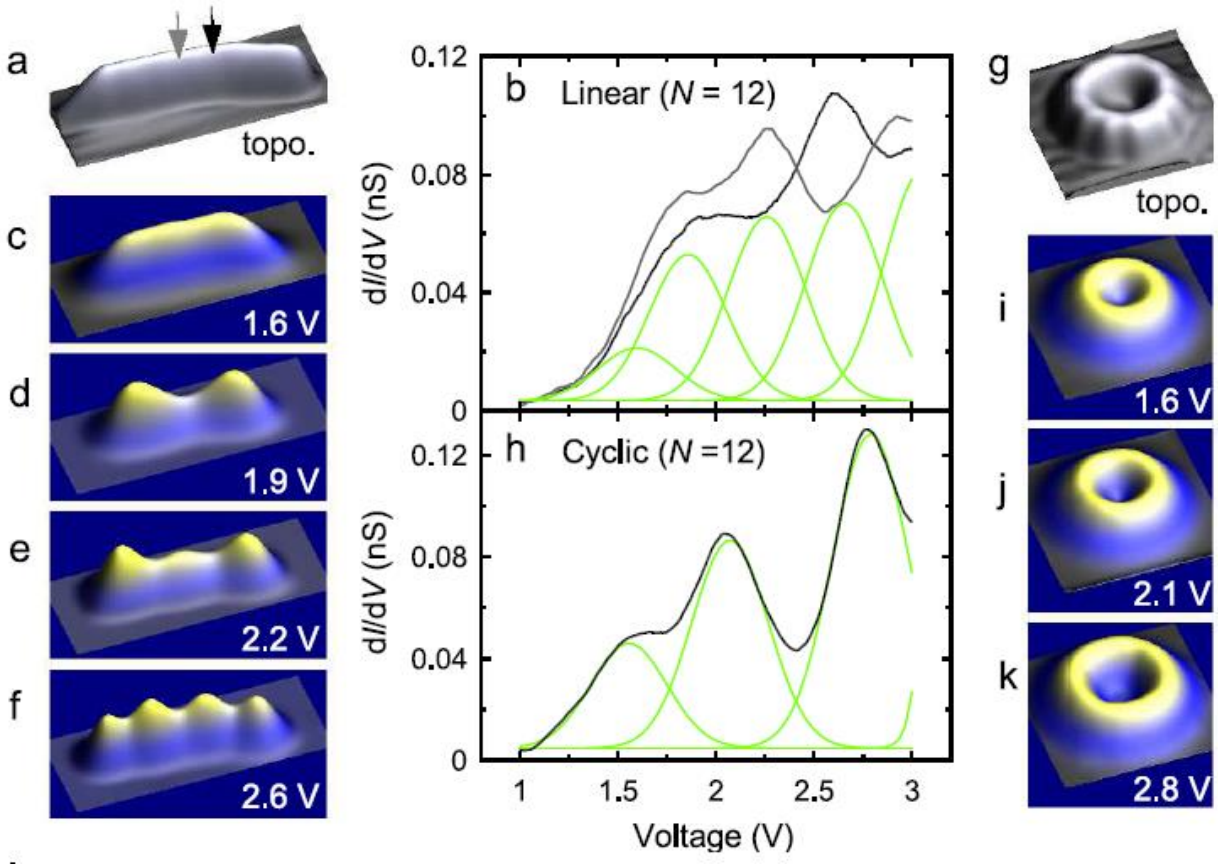

Figure 8 – (Color online) (a) Topographic STM image (I = 100 pA and V_{sample} = 0.1 V, 6.6 × 2.4 nm^2) and (b) constant height differential conductance spectra (set point: I = 5 pA and V_{sample} = 1 V) of a linear-[12]-thiophene. The grey and black spectra correspond to two positions of the tip on top of the wire (see grey and black arrows in (a)). Green lines are Gaussian function fits. (c) to (f) are constant height conductance maps acquired

at voltages corresponding to maxima in (b). The same data were acquired for a cyclo-[12]-thiophene: (g) topographic STM image (2.8 × 2.8 nm^2), (h) constant height differential conductance spectra acquired on top of the wire, and (i) to (k) constant height conductance maps acquired at voltages corresponding to maxima in (h)

1.3 WGM as Superpersistent Current

In the presence of random scatterings, e.g., due to classical chaos, Persistent Currents (PCs), one of the most intriguing manifestations of the Aharonov-Bohm (AB) effect, vanish for Schrödinger particles [7]. However, relativistic Dirac quantum AB rings threaded by a magnetic flux are extremely robust (superpersistent currents (SPCs)). A striking finding is that the SPCs can be attributed to a robust type of relativistic quantum states, i.e., Dirac whispering gallery modes (WGMs) that carry large angular momenta and travel along the boundaries and can potentially be the base for a new class of relativistic qubit systems.

By examining the eigenstates, we note that, for low energy levels, the Schrödinger particle is strongly localized throughout the domain, as shown in Figs. 9(a–c), since asymmetry in the domain geometry cause mixing angular momentum states and leading to localization of lower states in the entire domain region and vanishing AB oscillations. However, the Dirac fermion typically travels around the ring's boundaries, forming relativistic WGMs that persist under irregular boundary scattering due to chaos and are magnetic flux dependent, as shown in Fig. 9(d–f).

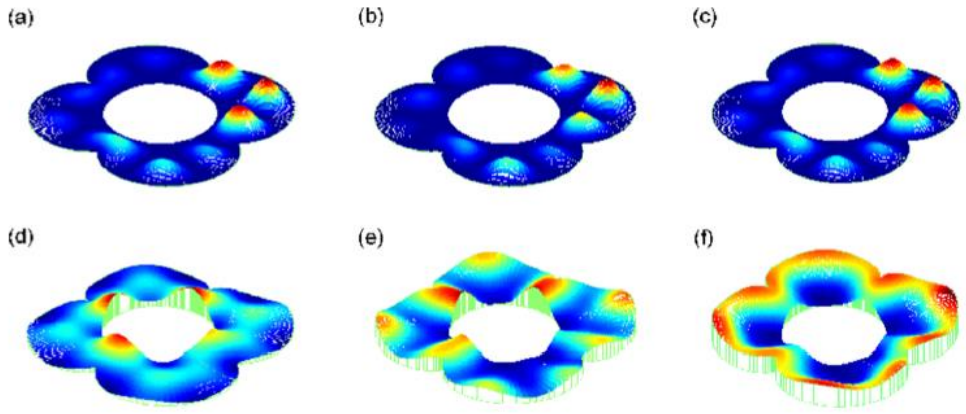

Figure 9 – Probability distribution of the 10th eigenstate for (a–c) nonrelativistic and (d–f) relativistic AB chaotic billiard, for different chaos degee [7]

1.4 Fabrication of Lateral Quantum Dot

Due to the vast application of self-organized *InP* quantum dots (QDs), especially in laser and single photon-source (SPS), they have been widely studied in the recent decades [9]. Self-organized *InP* quantum dots (QDs) grows on $Ga_xIn_{1-x}P$ lattice-matched to *GaAs* substrates (further denoted as *InP*/ *GaInP* QDs). Interestingly, *InP*/*GaInP* QDs have been shown to reveal Wigner Molecule (WM) states which make them an ideal candidate to be used in nano-electronics, quantum computing devices. Although, WM states could be observed in *InSb* nanowires, and carbon nanotubes. To this end, control of the QD's optical and structural properties is essential. For laser and SPS applications, the control of the properties of the QDs with sizes 40–70 *nm* have done, but not for larger *InP*/*GaInP* QDs (>100 nm) which is required for the optimization of WM structures.

In [9], the QD sample structure is as follows: 500 μm in direction [1 0 0] *GaAs* substrate misoriented by 2° or 6° towards the [1 1 0] direction, 50 *nm* thick *GaAs* buffer layer, 50 *nm* $Ga_xIn_{1-x}P$ latticed matched to the *GaAs* grown at 725 °C, seven monolayers of *InP* at 725 °C to form the QDs, and a 60 *nm* $Ga_xIn_{1-x}P$ cap layer grown at either 650 or 725 °C. Representative plan-view Transmission Electron Microscopy (TEM) images of the four samples are shown in figure 10 (a) as well as the lateral size probability density functions (PDFs). The QD lateral sizes range from ~100–200 *nm*. The PDFs peaked at 140, 160, 100, and 130 *nm* for samples i, ii, iii and iv, respectively.

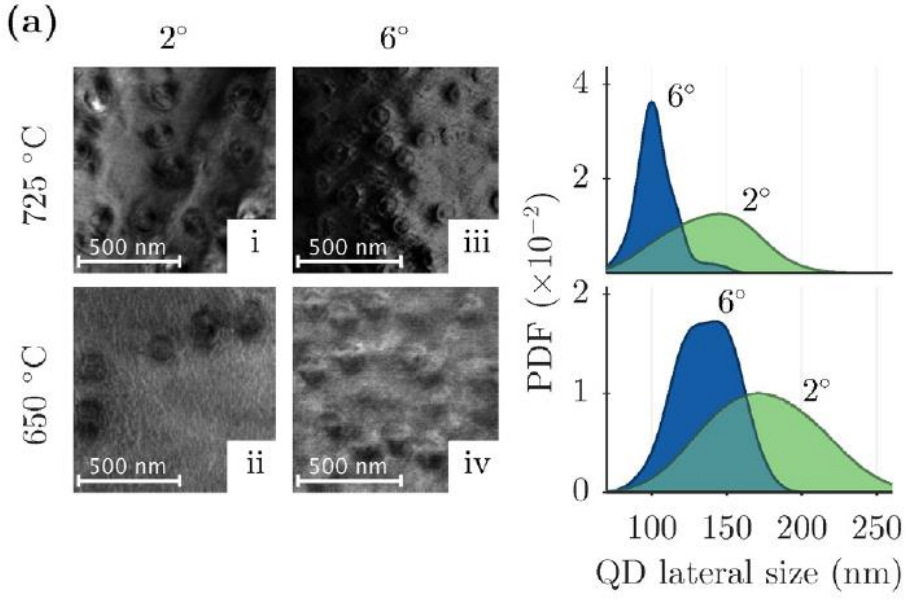

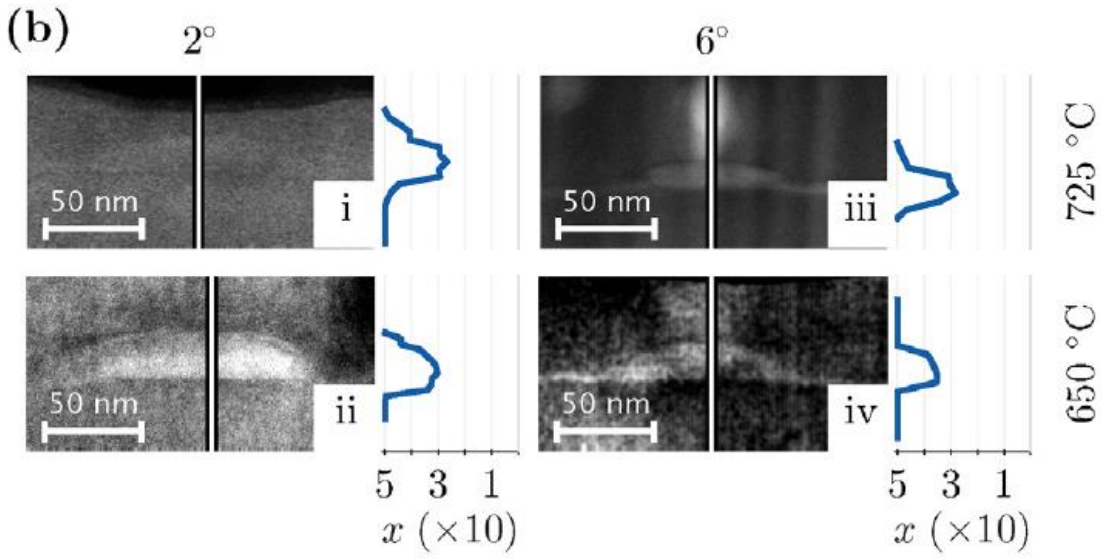

Figure 10 – Structural data of the samples i, ii, iii and iv: plan-view TEM images with the extracted lateral dot size probability distribution functions—(a) and cross-sectional TEM images and EDX scans—(b). The amount of $Ga_x(Ga_xIn_{1-x}P)$ for each line scan (along the vertical lines indicated) is shown to the image's right [9]

1.5 Wigner Localization and Conductance Anomalies

A Quantum Point Contact (QPC) is a constriction in the transverse direction which create a resistance for the electron motion where with applying voltage across the constriction, current can be induced. Hence, the QPC shows quantized conductance for different gate voltage, however, a shoulder like curve appear near the conductance $0.7G0=0.7*2e^2/h$ which cannot be explained by single particle approach. This anamoly is called '0.7 anomaly' or zero-bias peak called 'zero-bias anomaly' (ZBA).

Reference [12] observes repetitive splitting of the zero-bias anaomy by changing the distance of the scanning gate microscope tip, also appearing of 0.7 anomaly, simultaneously (Fig. 11).

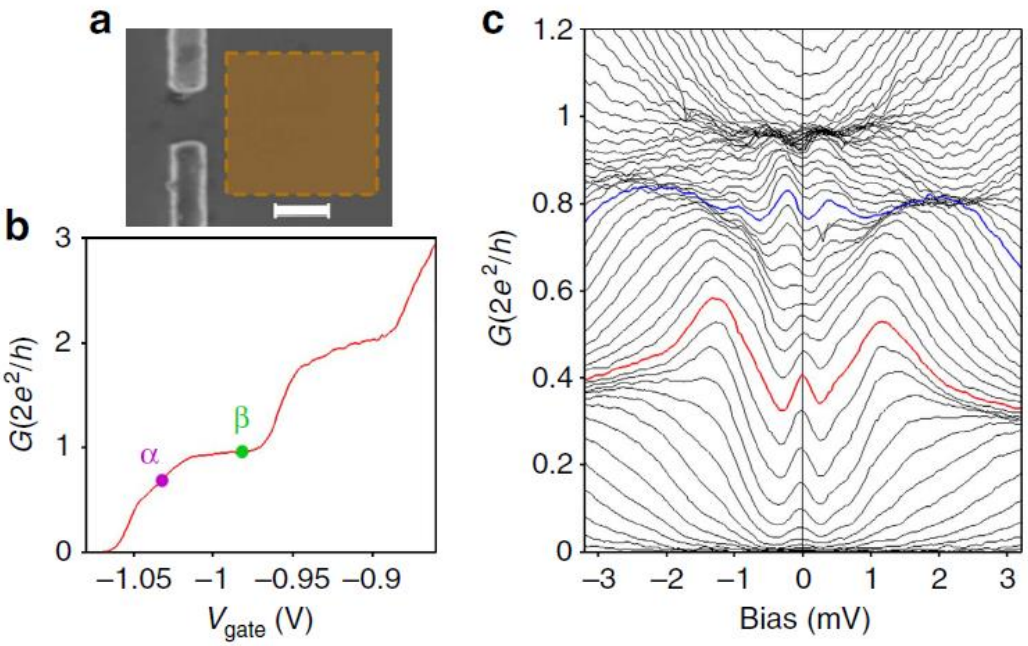

Figure 11 – Transport measurements. Base temperature is 20 mK. (a) Electron micrograph of the QPC gates. Scale bar, 300 *nm*. (b) Differential conductance *G* at zero bias versus split-gate voltage *V*gate. The 0.7 anomaly is visible below the first plateau. (c) Differential conductance *G* versus source-drain bias for different gate voltage *V*gate from -1.08 to -0.96 *V*

This behavior is explained as existing of Wigner localization containing charges with different parities, in which spin states in the channel shows alternating equilibrium and nonequilibrium Kondo screenings (Kondo effect can be explained as hybridization of localized electrons to the conduction electrons at low temperature which creates a narrow band gap).

This behavior can be interpreted in terms of alternating equilibrium and nonequilibrium Kondo screenings of different spin states localized in the channel. These alternating Kondo effects point towards the presence of a Wigner crystal containing several charges with different parities.

2 THEORETICAL APPROACH

2.1 Schrodinger Equation in Effective Mass Approximation

Schrodinger equation in effective mass approximation can be written as:

$$\left(-\frac{\hbar^2}{2}\nabla.(\frac{1}{m_e}\nabla)+V\right)\Psi = E\Psi \tag{10}$$

Regarding that, our structure is symmetric in azimuthal (φ) direction, by separation of variables, we can write wavefuntion as:

$$\Psi = \chi(r,z)\Theta(\varphi) \tag{11}$$

On the other hand, in cylinderical coordinates, the operator $\nabla.(\frac{1}{m_e}\nabla)$ is:

$$\nabla.(\frac{1}{m_e}\nabla) = \frac{1}{r}\frac{\partial}{\partial r}(\frac{1}{m_e}r\frac{\partial}{\partial r})+\frac{\partial}{\partial z}(\frac{1}{m_e}\frac{\partial}{\partial z})+\frac{1}{m_e r^2}\frac{\partial^2}{\partial\varphi^2} \tag{12}$$

By inserting Eqs. (11) and (12) into (10):

$$-\frac{h^2}{8\pi^2}\left[\frac{1}{r}\frac{\partial}{\partial r}(\frac{1}{m_e}r\frac{\partial\chi}{\partial r})+\frac{\partial}{\partial z}(\frac{1}{m_e}\frac{\partial\chi}{\partial z})\right]\Theta-\frac{h^2}{8\pi^2}\frac{\chi}{m_e r^2}\frac{\partial^2\Theta}{\partial\varphi^2}+V\chi\Theta = E\chi\Theta \tag{13}$$

where $\hbar = \frac{h}{2\pi}$. Deividing both sides of this equation by $\frac{\chi\Theta}{m_e r^2}$ gives:

$$-m_e r^2\frac{h^2}{8\pi^2}\frac{1}{\chi}\left[\frac{1}{r}\frac{\partial}{\partial r}(\frac{1}{m_e}r\frac{\partial\chi}{\partial r})+\frac{\partial}{\partial z}(\frac{1}{m_e}\frac{\partial\chi}{\partial z})\right]+m_e r^2(V-E) = \frac{h^2}{8\pi^2}\frac{1}{\Theta}\frac{\partial^2\Theta}{\partial\varphi^2} \tag{14}$$

Therefore, we can equate both side of the above equation to a constant like $-\frac{h^2}{8\pi^2}l^2$ which gives two independent equations as:

$$\frac{1}{\Theta}\frac{\partial^2\Theta}{\partial\varphi^2} = -l^2 \tag{15}$$

and

$$-m_e r^2\frac{h^2}{8\pi^2}\frac{1}{\chi}\left[\frac{1}{r}\frac{\partial}{\partial r}(\frac{1}{m_e}r\frac{\partial\chi}{\partial r})+\frac{\partial}{\partial z}(\frac{1}{m_e}\frac{\partial\chi}{\partial z})\right]+m_e r^2(V-E) = -\frac{h^2}{8\pi^2}l^2 \tag{16}$$

The solution of Eq. (15) is in the form:

$$\Theta = \exp(\pm il\varphi) \tag{17}$$

where due to the periodic condition $\Theta(\varphi+2\pi)=\Theta(\varphi)$, l, the principle quantum number, should be integer.

Furthermore, multiplying both sides of Eq. (16) with $\frac{\chi}{m_e r^2}$ and arranging the terms gives:

$$-\frac{h^2}{8\pi^2}\left[\frac{\partial}{\partial r}(\frac{1}{m_e}\frac{\partial\chi}{\partial r})+\frac{\partial}{\partial z}(\frac{1}{m_e}\frac{\partial\chi}{\partial z})\right]-\frac{h^2}{8\pi^2 m_e r}\frac{\partial\chi}{\partial r}+(V+\frac{h^2}{8\pi^2 m_e}\frac{l^2}{r^2})\chi=E\chi \tag{18}$$

which is in the form of a coefficient form partial differential equation (PDE):

$$\nabla.(-c\nabla u-\alpha u+\gamma)+au+\beta\nabla u=d_a\lambda u \tag{19}$$

with:

$$c=-\frac{h^2}{8\pi^2 m_e}\quad;\quad \beta_r=-\frac{h^2}{8\pi^2 m_e r}\quad;\quad a=V+\frac{h^2}{8\pi^2 m_e}\frac{l^2}{r^2}\quad;\quad d_a=1\quad;\quad \lambda=E \tag{20}$$

while other coefficients are zero.

We note that in Eq. (19), $\nabla=(\frac{\partial}{\partial r},\frac{\partial}{\partial z})$ is considered.

2.2 Evaluating the Effect of Coulomb Energy in Energy Spectra

To calculate Coulomb interaction between two electrons, the wavefunctions associated with these two electrons can be written as:

$$\psi(r_1,r_2)=c_1\psi_1(r_1)\psi_2(r_2)+c_2\psi_1(r_2)\psi_2(r_1) \tag{21}$$

where $\psi_1(r)$ and $\psi_2(r)$ are wavefunctions of two states, while r_1 and r_2 are positions of the electrons. The quantity $|c_1|^2$ is the propabibility of the electron with state $\psi_1(r)$ being in the position r_1 and electron with state $\psi_2(r)$ being in the position r_2. The similar definition stands for $|c_2|^2$. Therefore, c_1 and c_2 are equal to $\pm\frac{1}{\sqrt{2}}$, regarding that $|c_1|^2+|c_2|^2=1$ and $|c_1|^2=|c_2|^2$. Since electrons are fermions, the wavefunction of these two electrons should be antisymmetrized, hence, we choose $c_1=\frac{1}{\sqrt{2}}$ and $c_2=-\frac{1}{\sqrt{2}}$. Therefore, from Eq. (21):

$$\psi(r_1,r_2)=\frac{1}{\sqrt{2}}\psi_1(r_1)\psi_2(r_2)-\frac{1}{\sqrt{2}}\psi_1(r_2)\psi_2(r_1) \tag{22}$$

In fact, Eq. (22) is a representation of slater determinant, since this determinant can be decomposed to 2×2 determinants, and for studying two electrons, only the related 2×2 determinant would be kept and other components would be considered zero.

On the other hand, the potential energy between two-charge distribution can be calculated from:

$$dV=\frac{1}{4\pi\varepsilon_0\varepsilon_r}\frac{dq_1dq_2}{r_{12}} \tag{23}$$

where

$$dq_1dq_2=e^2\,|\psi(r_1,r_2)|^2\,dv_1dv_2=e^2\psi(r_1,r_2)^*\psi(r_1,r_2)dv_1dv_2 \tag{24}$$

Therefore,

$$V=\frac{e^2}{4\pi\varepsilon_0\varepsilon_r}\iint\frac{\psi^*(r_1,r_2)\psi(r_1,r_2)}{r_{12}}dv_1dv_2 \tag{25}$$

Inserting $\psi(r_1,r_2)$ from Eq. (22), one can obtain:

$$V=\frac{e^2}{4\pi\varepsilon_0\varepsilon_r}\iint\frac{|\psi_1(r_1)|^2|\psi_2(r_2)|^2}{r_{12}}dv_1dv_2-\iint\frac{\psi_1^*(r_1)\psi_2^*(r_2)\psi_1(r_2)\psi_2(r_1)}{r_{12}}dv_1dv_2 \tag{26}$$

where the first term:

$$V_d=\frac{e^2}{4\pi\varepsilon_0\varepsilon_r}\iint\frac{|\psi_1(r_1)|^2|\psi_2(r_2)|^2}{r_{12}}dv_1dv_2 \tag{27}$$

is called direct coulomb energy and

$$V_e=\iint\frac{\psi_1^*(r_1)\psi_2^*(r_2)\psi_1(r_2)\psi_2(r_1)}{r_{12}}dv_1dv_2 \tag{28}$$

is exchange coulomb energy.

2.3 Spin effect of the electrons in Coulomb interaction

Let's define the wavefunction of two correlated electrons as:

$$\chi(r_1,\omega_1,r_2,\omega_2)=\phi(r_1,r_2)\sigma(\omega_1,\omega_2) \tag{29}$$

where r_1 and r_2 are spatial parameters and ω_1 and ω_2 are spin parameters. The function $\chi(r_1,\omega_1,r_2,\omega_2)$ should be antisymmetrized. If the spins of the electrons are same, $\sigma(\omega_1,\omega_2)$ is symmetrized, therefore, $\phi(r_1,r_2)$ should be antisymmetrized (as Eq. 22). Therefore, by inserting this wavefunction in the Coulomb energy (Eq. 25), the exchange part of Coulomb energy would be negative. Vice versa, for different spin, $\phi(r_1,r_2)$ should be symmetrized and exchange coulomb interaction is positive.

However, according to another approach, we assume the wavefunction of an electron as:

$$\chi(r,\omega)=\phi(r)\sigma(\omega) \tag{30}$$

Let's calculate the notation $\langle\chi_i|\hat{h}|\chi_j\rangle$:

$$\langle\chi_i|\hat{h}|\chi_j\rangle=\int dr d\omega\chi_i^*(r,\omega)\hat{h}\chi_j(r,\omega) \tag{31}$$

Inserting Eq. (30) into (31):

$$\langle\chi_i|\hat{h}|\chi_j\rangle=\int dr d\omega\phi_i^*(r)\sigma_i^*(\omega)\hat{h}\phi_j(r)\sigma_j(\omega) \tag{32}$$

Separating spin function and spatial function gives:

$$\langle\chi_i|\hat{h}|\chi_j\rangle=\int d\omega\sigma_i^*(\omega)\sigma_j(\omega)\int dr\phi_i(r)\hat{h}\phi_j(r) \tag{33}$$

For same spin $\sigma_i=\sigma_j$

$$\int d\omega\sigma_i^*(\omega)\sigma_j(\omega)=1 \tag{34}$$

and for different spin, the integral is zero.

Therefore, to calculate single particle energy, we can write

$$\langle\chi_i|\hat{h}|\chi_i\rangle=\int d\omega\sigma_i^*(\omega)\sigma_i(\omega)\int dr\phi_i(r)\hat{h}\phi_j(r) \tag{35}$$

Therefore,

$$\langle\chi_i|\hat{h}|\chi_i\rangle=\int dr\phi_i(r)\hat{h}\phi_j(r) \tag{36}$$

For exchange coulomb inetraction, we can write:

$$[\chi_i\chi_j \mid \chi_j\chi_i] = \int dr_1 d\omega_1 dr_2 d\omega_2 \chi_i^*(r_1,\omega_1)\chi_j(r_1,\omega_1)\frac{1}{r_{12}}\chi_j^*(r_2,\omega_2)\chi_i(r_2,\omega_2) \tag{37}$$

With separating spin part and spatial parts:

$$[\chi_i\chi_j \mid \chi_j\chi_i] = \left[\int d\omega_1 \sigma_i^*(\omega_1)\sigma_j(\omega_1)\right]\left[\int d\omega_2 \sigma_j^*(\omega_2)\sigma_i(\omega_2)\right]\left[\int dr_1 dr_2 \phi_i^*(r_1)\phi_j(r_1)\frac{1}{r_{12}}\phi_j^*(r_2)\phi_i(r_2)\right] \tag{38}$$

Therefore, for different spin $\sigma_i \neq \sigma_j$, the integral is zero. However, for direct coulomb interaction, we can write:

$$[\chi_i\chi_i \mid \chi_j\chi_j] = \left[\int d\omega_1 \sigma_i^*(\omega_1)\sigma_i(\omega_1)\right]\left[\int d\omega_2 \sigma_j^*(\omega_2)\sigma_j(\omega_2)\right]\left[\int dr_1 dr_2 \phi_i^*(r_1)\phi_i(r_1)\frac{1}{r_{12}}\phi_j^*(r_2)\phi_j(r_2)\right] \tag{39}$$

Regardless of same or different spins, we can write:

$$[\chi_i\chi_i \mid \chi_j\chi_j] = \int dr_1 dr_2 \phi_i^*(r_1)\phi_i(r_1)\frac{1}{r_{12}}\phi_j^*(r_2)\phi_j(r_2) \tag{40}$$

According to this approach, for same spin, exchange coulomb energy is negative, and for different spin, it is zero. In our calculations, we have used the second approach.

2.4 Fock-operator

The energy associated to an electronic system can be defined as:

$$E^{HF} = \sum_i \langle \chi_i \mid h \mid \chi_i \rangle + \frac{1}{2}\sum_{ij}[\chi_i\chi_i \mid \chi_j\chi_j] - [\chi_i\chi_j \mid \chi_j\chi_i] \tag{41}$$

where the first, second and third terms are single particle energy, direct coulomb energy and exchange coulomb energy. The coefficient $1/2$ is due to the fact that in the sum of electron interactions, each electrons has considered twice. However, currently we do not care about coefficients and sign, since later, we can adjust them regarding the number and spin of the electrons in the orbitals.

Let's assume wavefunction of orbital ith (χ_i) changes a bit as:

$$\chi_i \rightarrow \chi_i + \delta\chi_i \tag{42}$$

Langragian of this orbital can be defined as:

$$L\{\chi_i\} = E^{HF}\{\chi_i\} - \sum_{ij}\varepsilon_{ij}(\langle \chi_i \mid \chi_j \rangle - \delta_{ij}) \tag{43}$$

In fact Eq. (43) investigate the orthogonality of the orbitals. The unknown coefficients (Langragian multiplier) ε_{ij} can be found by differentiating of Eq. (43) and equating it to zero.

The differentiation of the Langragian defined in Eq. (43) is:

$$\delta L\{\chi_i\} = \delta E^{HF}\{\chi_i\} - \sum_{ij} \varepsilon_{ij} \delta\langle \chi_i \mid \chi_j \rangle \tag{44}$$

where the differentiation of the term $\langle \chi_i \mid \chi_j \rangle$ is:

$$\delta\langle \chi_i \mid \chi_j \rangle = \langle \delta\chi_i \mid \chi_j \rangle + \langle \chi_i \mid \delta\chi_j \rangle \tag{45}$$

and differentiation of E^{HF} from Eq. (41) is:

$$\begin{aligned}
\delta E^{HF} &= \sum_i \left(\langle \delta\chi_i \mid \hat{h} \mid \chi_i \rangle + \langle \chi_i \mid \hat{h} \mid \delta\chi_i \rangle \right) \\
&+ \frac{1}{2} \sum_{ij} [\delta\chi_i \chi_i \mid \chi_i \chi_i] + [\chi_i \delta\chi_i \mid \chi_i \chi_i] + [\chi_i \chi_i \mid \delta\chi_i \chi_i] + [\chi_i \chi_i \mid \chi_i \delta\chi_i] \\
&- \frac{1}{2} \sum_{ij} [\delta\chi_i \chi_j \mid \chi_j \chi_i] + [\chi_i \delta\chi_j \mid \chi_j \chi_i] + [\chi_i \chi_j \mid \delta\chi_j \chi_i] + [\chi_i \chi_j \mid \chi_j \delta\chi_i]
\end{aligned} \tag{46}$$

If we consider the integral form of Eq. (46), we can observe that some terms in this equation are equal to each other, and it can written as:

$$\begin{aligned}
\delta E^{HF} &= \sum_i \left(\langle \delta\chi_i \mid \hat{h} \mid \chi_i \rangle + \langle \chi_i \mid \hat{h} \mid \delta\chi_i \rangle \right) \\
&+ \sum_{ij} [\delta\chi_i \chi_i \mid \chi_i \chi_i] + [\chi_i \delta\chi_i \mid \chi_i \chi_i] - \sum_{ij} [\delta\chi_i \chi_j \mid \chi_j \chi_i] + [\chi_i \delta\chi_j \mid \chi_j \chi_i]
\end{aligned} \tag{47}$$

By inserting Eqs. (45) and (47) into (44), we can write:

$$\begin{aligned}
\delta L\{\chi_i\} &= \sum_i \left(\langle \delta\chi_i \mid \hat{h} \mid \chi_i \rangle + \langle \chi_i \mid \hat{h} \mid \delta\chi_i \rangle \right) \\
&+ \sum_{ij} [\delta\chi_i \chi_i \mid \chi_i \chi_i] + [\chi_i \delta\chi_i \mid \chi_i \chi_i] - \sum_{ij} [\delta\chi_i \chi_j \mid \chi_j \chi_i] + [\chi_i \delta\chi_j \mid \chi_j \chi_i] \\
&- \sum_{ij} \varepsilon_{ij} (\langle \delta\chi_i \mid \chi_j \rangle + \langle \chi_i \mid \delta\chi_j \rangle)
\end{aligned} \tag{48}$$

Some terms of Eq. (48) is complex conjugate of each other, therefore, this equation can be written as:

$$\delta L\{\chi_i\} = \sum_i \langle \delta\chi_i \mid \hat{h} \mid \chi_i \rangle + \sum_{ij} [\delta\chi_i \chi_i \mid \chi_i \chi_i] - \sum_{ij} [\delta\chi_i \chi_j \mid \chi_j \chi_i] - \sum_{ij} \varepsilon_{ij} \langle \delta\chi_i \mid \chi_j \rangle + complex.conjugate \quad (49)$$

We can write Eq. (49) in the integral form as:

$$\delta L\{\chi_i\} = \sum_i \int d\vec{r}_1 \delta\chi_i^*(\vec{r}_1) \left[\begin{array}{l} \hat{h}(\vec{r}_1)\chi_i(\vec{r}_1) + \sum_j \chi_i(\vec{r}_1) \int d\vec{r}_2 \frac{1}{r_{12}} \chi_j^*(\vec{r}_2)\chi_j(\vec{r}_2) - \sum_j \chi_j(\vec{r}_1) \int d\vec{r}_2 \frac{1}{r_{12}} \chi_j^*(\vec{r}_2)\chi_i(\vec{r}_2) \\ -\sum_j \varepsilon_{ij}\chi_j(\vec{r}_1) \end{array} \right] + c.c = 0 \quad (50)$$

In order that Eq. (50) being equal to zero, the expression in the bracket should be zero:

$$\hat{h}(\vec{r}_1)\chi_i(\vec{r}_1) + \sum_j \left[\int d\vec{r}_2 \frac{1}{r_{12}} \chi_j^*(\vec{r}_2)\chi_j(\vec{r}_2) \right] \chi_i(\vec{r}_1) - \sum_j \left[\int d\vec{r}_2 \frac{1}{r_{12}} \chi_j^*(\vec{r}_2)\chi_i(\vec{r}_2) \right] \chi_j(\vec{r}_1) = \sum_j \varepsilon_{ij}\chi_j(\vec{r}_1) \quad (51)$$

In Eq. (51), we can define operators $\hat{J}_j$ and $\hat{K}_j$ which are related to the direct and exchange coulomb interaction, respectively:

$$\hat{J}_j \chi_i(\vec{r}_1) = \int d\vec{r}_2 \frac{1}{r_{12}} \chi_j^*(\vec{r}_2)\chi_j(\vec{r}_2)\chi_i(\vec{r}_1) \quad (52)$$

$$\hat{K}_j \chi_i(\vec{r}_1) = \int d\vec{r}_2 \frac{1}{r_{12}} \chi_j^*(\vec{r}_2)\chi_i(\vec{r}_2)\chi_j(\vec{r}_1) \quad (53)$$

Therfore, Eq. (51) can be written in the operator form as:

$$\left(\hat{h} + \sum_j \hat{J}_j - \sum_j \hat{K}_j \right) \chi_i(\vec{r}_1) = \sum_j \varepsilon_{ij}\chi_j(\vec{r}_1) \quad (54)$$

We choose Langragian multiplier ε_{ij} to be diagonal ($\varepsilon_{ij} = 0; i \neq j$), therefore, Eq. (54) can be written as:

$$\left(\hat{h} + \sum_j \hat{J}_j - \sum_j \hat{K}_j \right) \chi_i(\vec{r}_1) = \varepsilon_{ii}\chi_i(\vec{r}_1) \quad (55)$$

3 METHODS AND RESULTS

3.1 4 meV QD

3.1.1 Energy Spectra

The eigenvalues (eigenenergies) and eigenfunctions of Eq. (19) with coefficients defined in Eq. (20) can be evaluated by Finite Element Method by Comsol software, "Coefficient Form PDE" section. To obtain eigenenergies in eV unit, we can divide h and m_e in Eq. (20) by the charge of electron e. The Quantum Dot (QD) and surrounding areas are InP and $GaAs$ with effective mass of electrons $0.08m_e$ and $0.067m_e$, respectively while the applied potential on the QD is 0 and on the surrounding area is $0.2\,eV$. Therefore, In Comsol, two PDE are defined, one of them for QD and another one for sorrounding area. Although the height of QD is too small, it should be considered as a 3D structure in order to achieve a more accurate results, since some energy degeneracy would be created due to the non-zero height of the QD.

In order to achieve a precise result, a dense meshing is considered for the structure as shown in Fig. 12 (a). Figure 12 (b) shows energy spectrum of a QD for which its dimensions is adjusted in order to achieve $4\,meV$ energy splitting between two lowest energy levels, s and p.

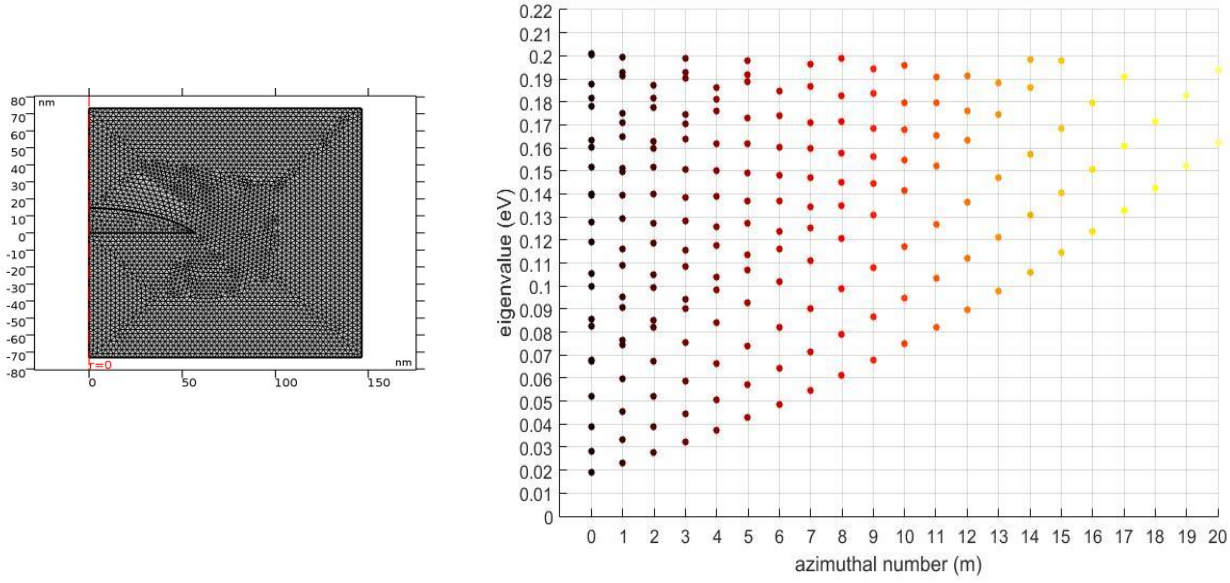

Figure 12 - (a) Meshing. (b) Energy Spectrum for QD with 4 meV s-p energy splitting

This figure shows some energy degeneracy for each azimuthal number (m).

3.1.2 Wavefunction

The wavefuncions of the QD (Figure 13) shows that these degeneracy is due to the changing the quantum number associated to the height of the QD (z-direction). It starts between 5th and 6th eigenvalues and the splitting increases with increasing the azimuthal number.

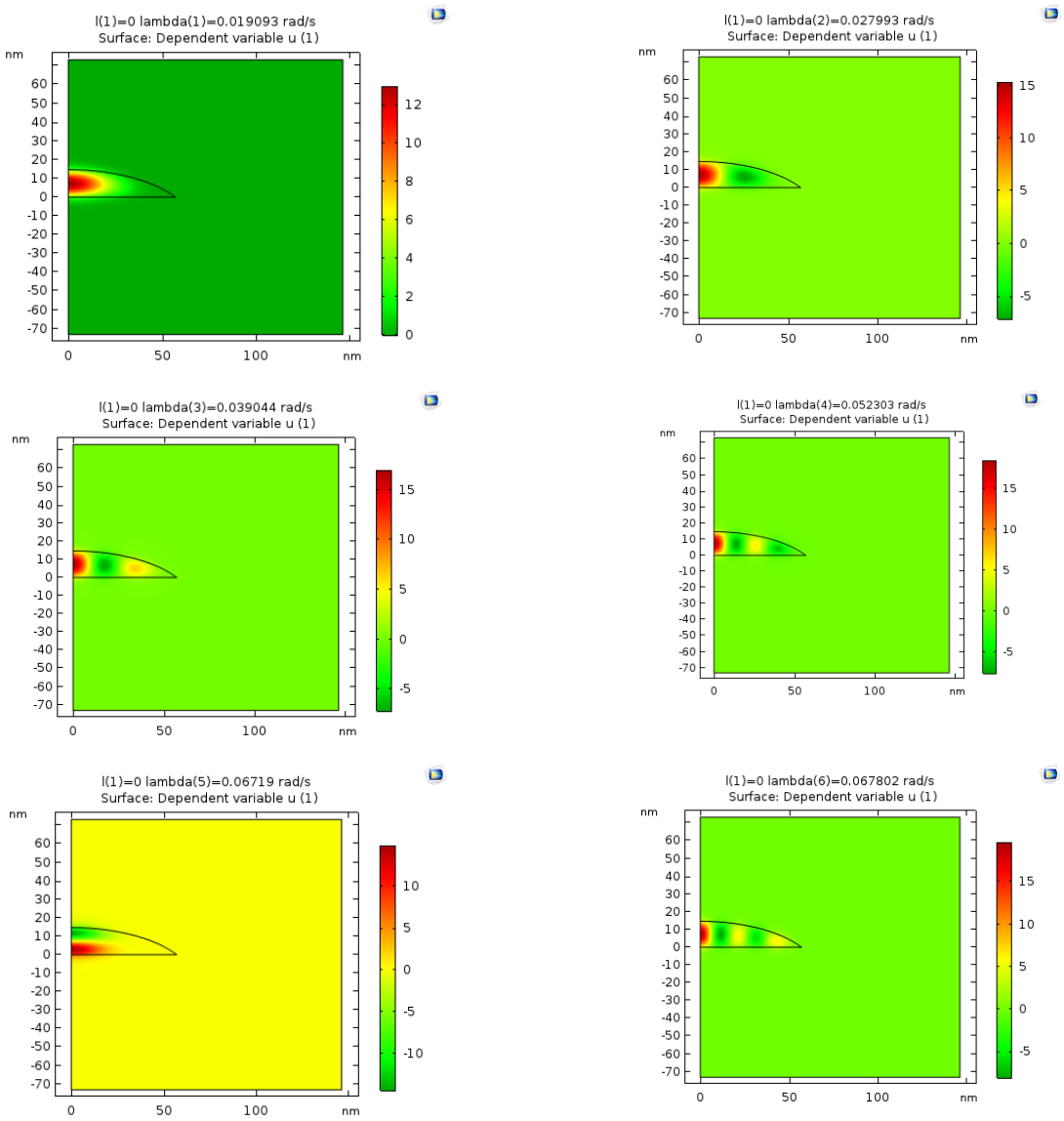

Figure 13 - Eigenfunctions of $4\,meV$ QD for azimuthal numbers $m = 0$

3.1.3 WGMs

The probability densities ($|\psi|^2$) of some of the Whispering Gallery Modes (WGMs) is also depicted in Figure 15.

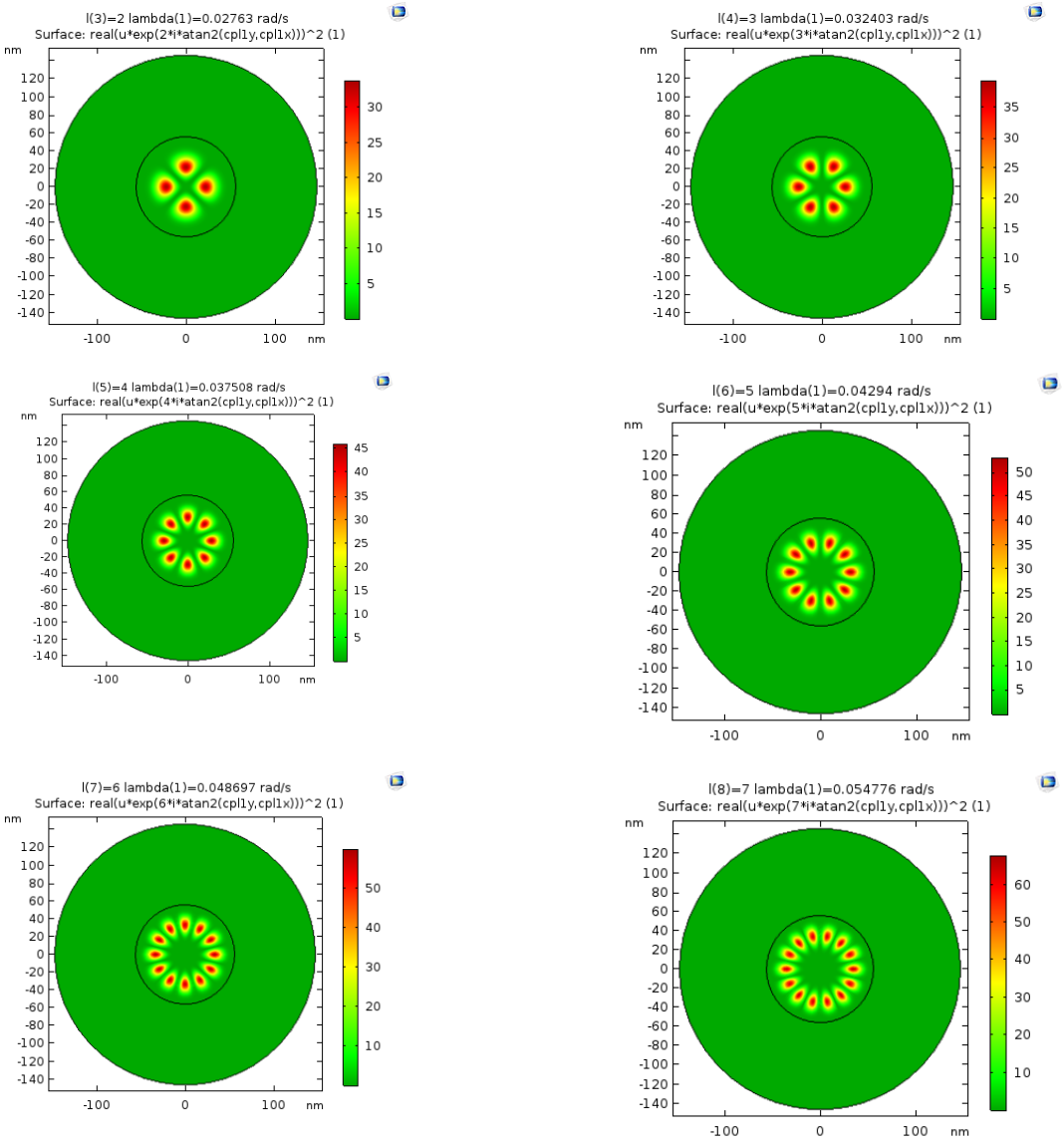

Figure 14 - Probability densities of WGMs for $m=2$ to $m=7$

3.2 2 meV QD

3.2.1 Energy Spectra and Wavefunctions

With changing the size of the QD, its energy spectrum can be manipulated. Figure 15, shows energy spectrum of a QD for which its size is adjusted in order to create $2\,meV$ energy splitting between s & p-states. It shows that energy spectrum is denser comparing to $4\,meV$ QD, and its wavefunctions depicted in Fig. 16 shows that

energy degeneracy starts between 4th and 5th eigenvalues (instead of 5th and 6th in 4 *meV* QD).

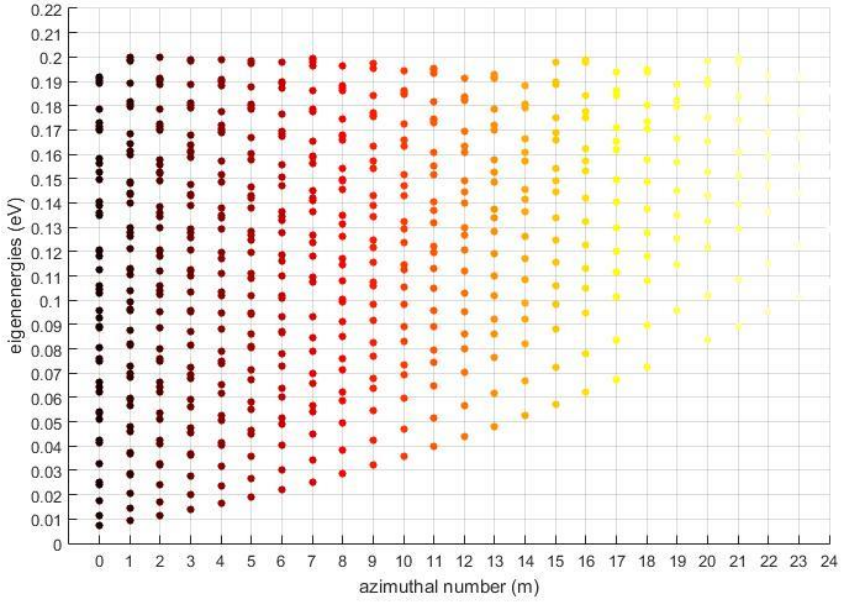

Figure 15 - Energy spectrum of 2 *meV* QD

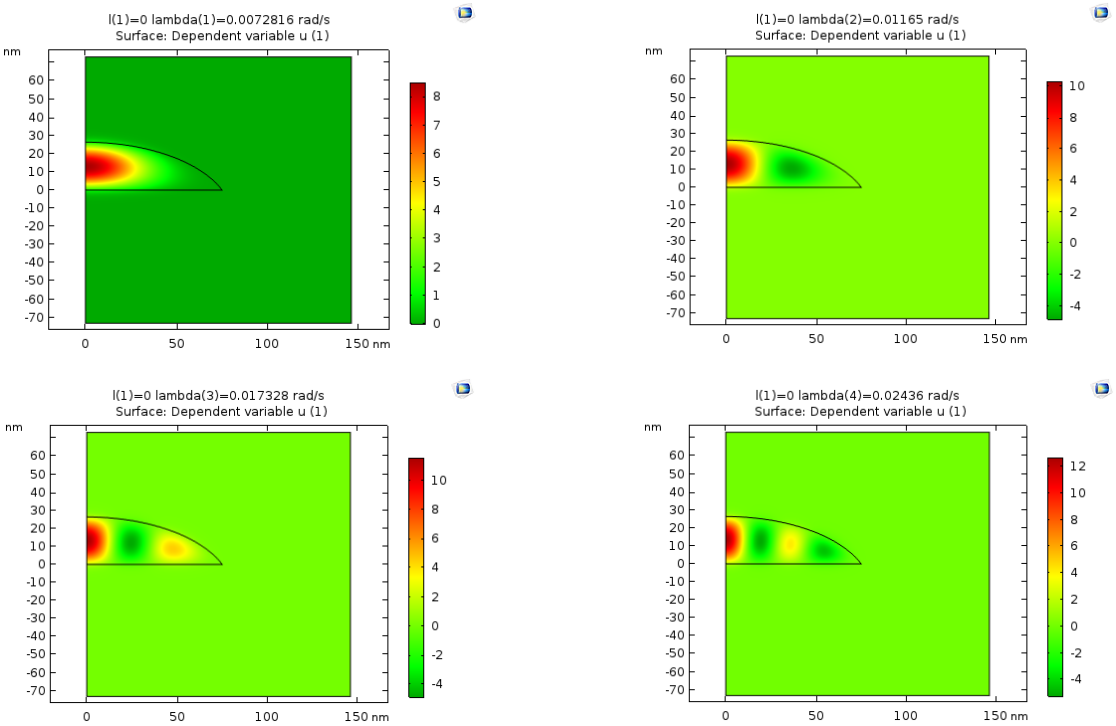

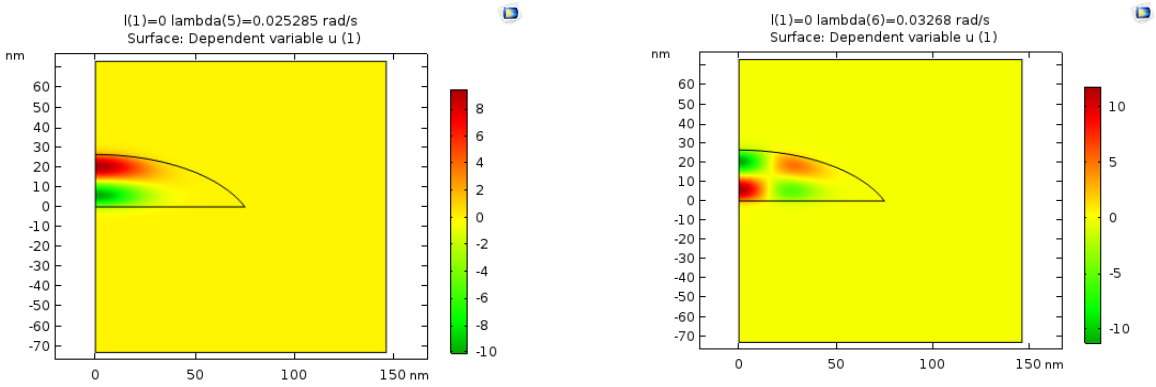

Figure 16 - Eigenfunctions of $2meV$ QD for azimuthal numbers $m=0$

3.3 Effect of Coulomb Interaction

We assume a QD which contain 5 electrons in ground state and also one electorn in the excited state or 4 electrons in the ground state and 2 electrons in the excited state. Therefore, to evaluate Coulomb interaction, different arrangements are considered (Fig. 18).

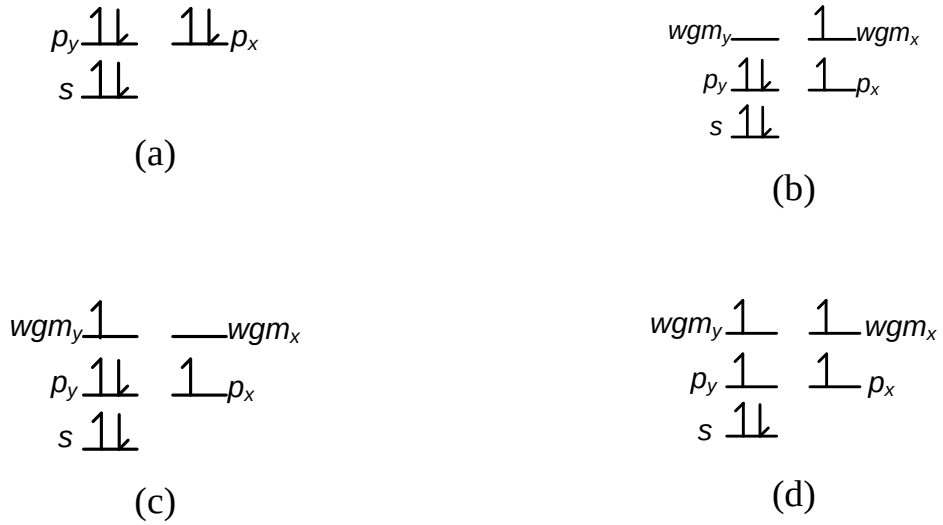

Figure 17 - Different arrangement of 6 electrons in the QD

In Fig. 17a, coulomb energy of one of the electron in p_x orbital is

$$C_1=[p_xp_x]+[2p_xp_y-(p_xp_y)_e]+[2sp_x-(sp_x)_e] \tag{56}$$

where p_xp_x is direct coulomb interaction between two electrons in p_x state, which can be evaluated from Eq. (27). The term p_xp_y is direct Coulomb interaction between one

electron in p_x state and two electrons in p_y state (therefore, it has coefficient 2) and $(p_x p_y)_e$ is exchange Coulomb interaction between these electrons, since the electron under study in p_x has same spin with one of the electrons in (p_x has φ dependent as $\cos(m\varphi)$ while p_y has $\sin(m\varphi)$). The same condition is considered for the other states. In Fig. 18b, coulomb energy of the electron in wgm_x is

$$C_2 = [p_x wgm_x - (p_x wgm_x)_e] + [2p_y wgm_x - (p_y wgm_x)_e] + [2swgm_x - (swgm_x)_e] \quad (57)$$

The calculated Coulomb energy difference between Figs. 18a and 18b is $C_1 - C_2 = 5.93\,meV$.

If we consider the arrangemnet of Fig. 18c (excited electron in wgm_y), the Coulomb energy difference between Figs. 18c and 18a is calculated $5.7\,meV$.

For two electron in wgm orbital (Fig. 18d), the coulomb energy difference between Figs. 18d and 18a is calculated $15.15\,meV$, therefore, we can expect that each of the electrons in wgm has about $15.15/2 = 7.58\,meV$ lower energy than the electron in p orbital.

With excitation of an electron, a s- hole would be created in the structure, hence, the effect of exiton energy should also be added in the Coulomb interaction. The s-hole wavefunction is obtained by considereng effective mass of hole $m = 0.6m_e$.

The exiton energy beween s-hole and an electron in p_x orbital is calculated $s_h p_x = 7.75\,meV$ while for $wgm_x(m=2)$, it is $s_h wgm_x = 6.3\,meV$, therefore, the value $7.75 - 6.3 = 1.45\,meV$ should also be added to the coulomb energy difference between Figs. 18a and 18b.

For the other states, the difference of the Coulomb interaction can be calculated, similarly. We assume first eigenstates of azimuthal number $m = 2, 3, \ldots$ as wgm, the second eigenstates of $m = 0, 1, 2, \ldots$ as xII, and third eigenstates of $m = 0, 1, 2, \ldots$ as $xIII$.

Figure 19a shows, energy spectra for one electron in the excited state (Fig. 18b) with taking into account the Coulomb interaction between the electrons, while in Fig. 19b exitonic energy is also included.

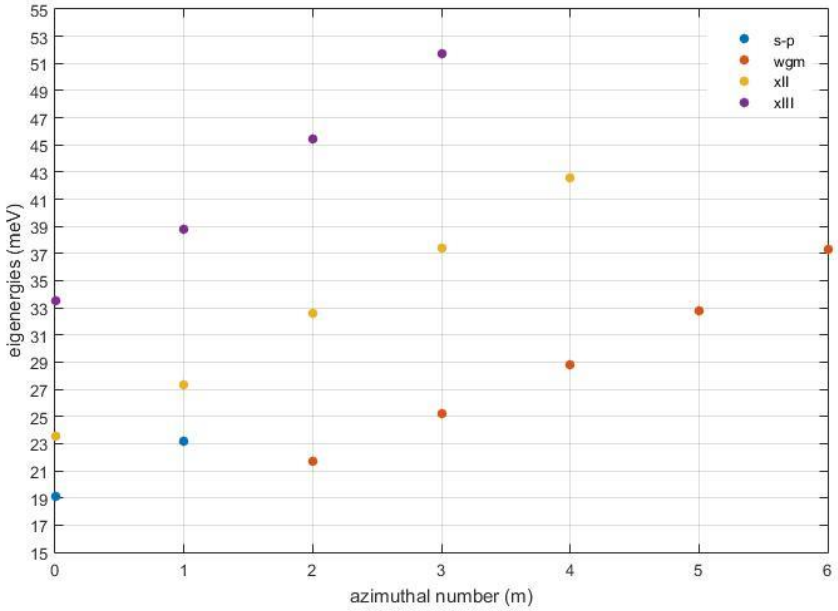

(a)

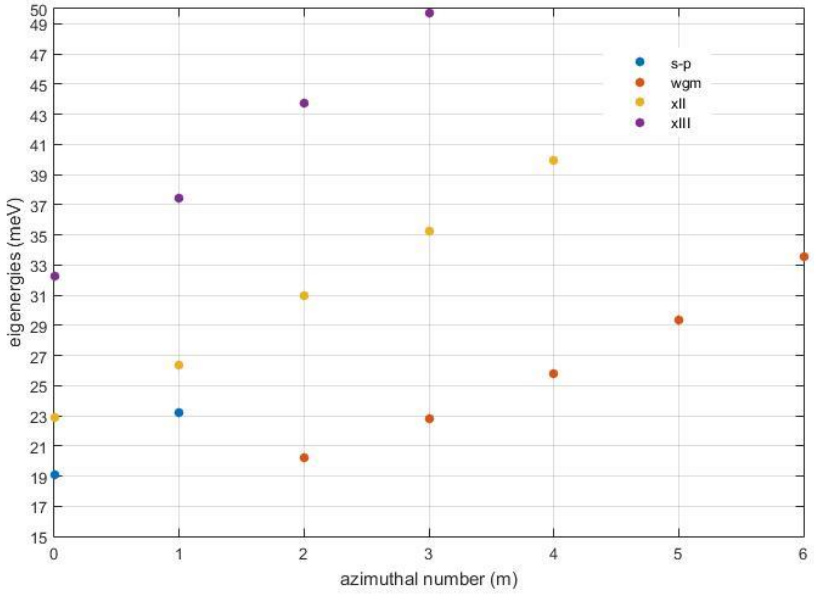

(b)

Figure 18 - Energy spectra for one electron in the excited state: (a) without excitonic energy. (b) with exitonic energy

Fig. 19 is related to the energy spectra for 2 electrons in the excited state (Fig. 17d).

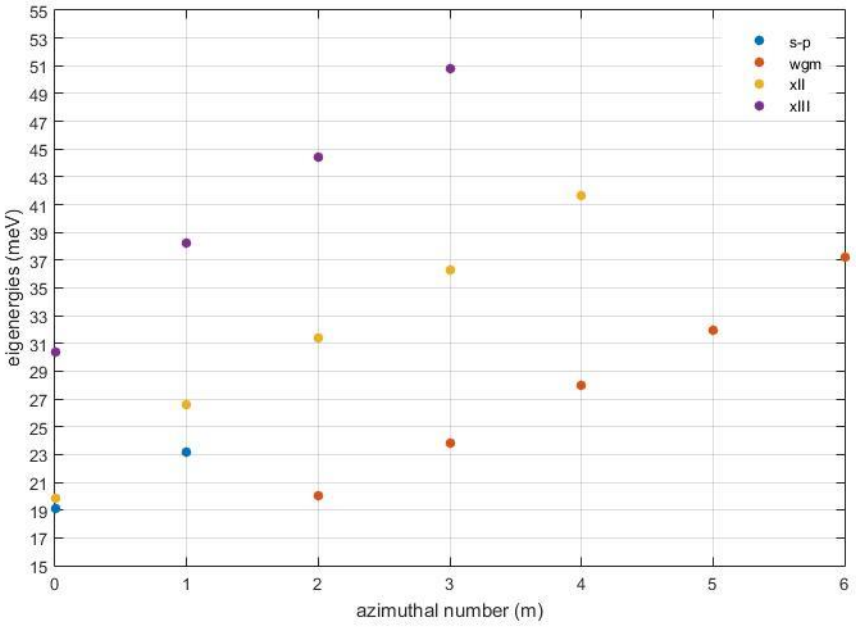

(a)

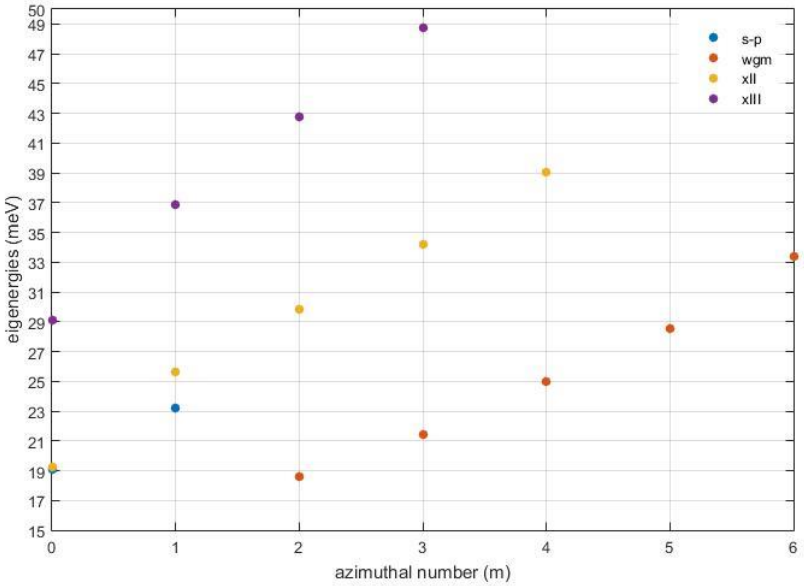

(b)

Figure 19 - Energy spectra for 2 electron in the excited state: (a) without exitonic energy. (b) with exitonic energy

3.4 Variational Method (Hartree-Fock Approach)

In this section we evaluate the result with variational (Hartree-Fock (HF)) method. Energy of an electron in state χ_i can be calculated from Fock-operator as:

$$\left(\hat{h}+\sum_j \hat{J}_j-\sum_j \hat{K}_j\right)\chi_i(\vec{r}_1)=\varepsilon_{ii}\chi_i(\vec{r}_1) \tag{58}$$

The general concept is that the shape of orbitals deviate a bit from their single particle wavefunctions due to the interaction between the orbitals. Therefore, the new wavefunction can be written as a linear combination of all the orbitals (in order to take into account their interactions) and estimate their new energy and wavefunction by variational method.

Equation (58) is an eigenvalue problem which gives wavefuncion and energy of i th orbital. First, we should choose eigenbasis, and write wavefunction of the orbitals as a linear combination of these eigenbasis. It is more convenient to use single particle wavefunctions as the eigenbasis, since they are currently available. If we consider single particle wavefunction, equivalent to atomic orbital and the wavefunction under study χ_i, equivalent to molecular orbital, this method is called Molecular Orbital as a Linear Combination of Atomic Orbital (MO-LCAO) method.

For our structure, we assume ground states have the wavefunction as their single particle states, but the excited state, as a linear combination of the single particle wavefunctions. For instance, for WGM with azimuthal number $m=2$ we can write:

$$WGM=c_1 s+c_2 p_y+c_3 p_x+c_4 wgm_x \tag{59}$$

By inserting Eq. (59), into (58):

$$\left(\hat{h}+\sum_j \hat{J}_j-\sum_j \hat{K}_j\right)\left(c_1 s(\vec{r}_1)+c_2 p_y(\vec{r}_1)+c_3 p_x(\vec{r}_1)+c_4 wgm(\vec{r}_1)\right)=\varepsilon_{ii}\left(c_1 s(\vec{r}_1)+c_2 p_y(\vec{r}_1)+c_3 p_x(\vec{r}_1)+c_4 wgm(\vec{r}_1)\right) \tag{60}$$

where, ε_{ii} is the energy of orbital WGM. In this equation $j=1,2,3$ is related to the orbitals s, p_y, p_x, respectively. The operators $\vec{J}_1$ and $\vec{K}_1$ are related to the direct and exchange coulomb interation of orbital $s(\vec{r})$ and $WGM(\vec{r})$, and we can write:

$$\vec{J}_1\left(WGM(\vec{r}_1)\right) = 2\int d\vec{r}_2 . s(\vec{r}_2)^* s(\vec{r}_2)\frac{1}{r_{12}} WGM(\vec{r}_1) \tag{61}$$

$$\vec{K}_1\left(WGM(\vec{r}_1)\right) = -\int d\vec{r}_2 . s(\vec{r}_2)^* s(\vec{r}_1)\frac{1}{r_{12}} WGM(\vec{r}_2) \tag{62}$$

In Eq. (61), the coefficient 2 is due to the direct coulomb effect of 2 electrons in s orbital on WGM orbital. The minus sign in Eq. (62) is due to the one electron in $s(\vec{r})$ orbital which has same spin with the electron in $WGM(\vec{r})$ orbital.

For the coulomb operator of $p_y(\vec{r})$ orbital on $WGM(\vec{r})$, we can write:

$$\vec{J}_2\left(WGM(\vec{r}_1)\right) = 2\int d\vec{r}_2 . p_y(\vec{r}_2)^* p_y(\vec{r}_2)\frac{1}{r_{12}} WGM(\vec{r}_1) \tag{63}$$

$$\hat{K}_2\left(WGM(\vec{r}_1)\right) = -\int d\vec{r}_2 . p_y(\vec{r}_2)^* p_y(\vec{r}_1)\frac{1}{r_{12}} WGM(\vec{r}_2) \tag{64}$$

The coulomb operator of $p_x(\vec{r})$ orbital on $WGM(\vec{r})$ is:

$$\hat{J}_3\left(WGM(r_1)\right) = \int d\vec{r}_2 . p_x(\vec{r}_2)^* p_x(\vec{r}_2)\frac{1}{r_{12}} WGM(\vec{r}_1) \tag{65}$$

$$\vec{K}_3\left(WGM(\vec{r}_1)\right) = -\int d\vec{r}_2 . p_x(\vec{r}_2)^* p_x(\vec{r}_1)\frac{1}{r_{12}} WGM(\vec{r}_2) \tag{66}$$

regarding that there is one electron in $p_x(\vec{r})$ orbital with the same spin as the electron in $WGM(\vec{r})$ orbital.

Since there are four unknown parameters c_1, c_2, c_3, c_4 , four equations are needed to calculate them. According to Roothan method, first equation can be obtained by multiplying both sides of Eq. (60) by $< s(\vec{r}_1)|$ (multiplying it by $s^*(\vec{r}_1)$ and taking integral with respect to $\vec{r}_1$). Similarly, second, third and fourth equation can be obtained by multiplying it by $< p_y(\vec{r}_1)|$, $< p_x(\vec{r}_1)|$, $< wgm(\vec{r}_1)|$, respectively. From these four equations,

we can arrange the terms with respect to the unknown coefficients c_1, c_2, c_3, c_4, which yields the matrix form equation as:

$$\begin{bmatrix} F_{11} & F_{12} & F_{13} & F_{14} \\ F_{21} & F_{22} & F_{23} & F_{24} \\ F_{31} & F_{32} & F_{33} & F_{34} \\ F_{41} & F_{42} & F_{43} & F_{44} \end{bmatrix} \begin{bmatrix} c_1 \\ c_2 \\ c_3 \\ c_4 \end{bmatrix} = \varepsilon_{ii} \begin{bmatrix} S_{11} & S_{12} & S_{13} & S_{14} \\ S_{21} & S_{22} & S_{23} & S_{24} \\ S_{31} & S_{32} & S_{33} & S_{34} \\ S_{41} & S_{42} & S_{43} & S_{44} \end{bmatrix} \begin{bmatrix} c_1 \\ c_2 \\ c_3 \\ c_4 \end{bmatrix} \tag{67}$$

where due to the large expressions, it is shown parametrically. Equation (67) can be written as:

$$\underline{\underline{S}}^{-1}\underline{\underline{F}}\underline{\underline{C}} = \varepsilon_{ii}\underline{\underline{C}} \tag{68}$$

which is an eigenvalue problem. The eigenvalues and eigenvectors of the matrix $\underline{\underline{S}}^{-1}\underline{\underline{F}}$ gives ε_{ii} and $\underline{\underline{C}}$, respectively (we note that if we choose the ground states as a linear combination of the eigenbasis either, then the operators would also contain the unknown coefficients $\underline{\underline{C}}$, therefore the problem would be Self-Consistent Field (SCF), since the operators depend on the eigenfunctions, however, our case is not self-consistent).

The calculated eigenvalues and eigenvectors are according to:

$$\begin{aligned} &E_1 = 53.6070\,;\, V_1 = \left(0.1494,\, 0,\, 0.0149,\, -0.9887\right) \\ &E_2 = 44.6968\,;\, V_2 = \left(0.9868,\, 0,\, 0.0631,\, 0.1490\right) \\ &E_3 = 46.0224\,;\, V_3 = \left(-0.0022,\, 0,\, -1,\, 0.0068,\, \right) \\ &E_4 = 48.2944\,;\, V_4 = \left(0,\, 1,\, 0,\, 0\right) \end{aligned} \tag{69}$$

where we choose the first eigenvalue and eigenvector, since c_4 (coefficient of wgm_x in Eq. (59)) is near one.

It may also be reasonable to investigate five eigenbasis:

$$WGM = c_1 s + c_2 p_y + c_3 p_x + c_4 wgm_x + c_5 wgm_y \tag{70}$$

in order to observe the difference of energy levels of WGM_x and WGM_y.

The calculated eigenvalues and eigenvectors are as below:

$$\begin{aligned} &E_1 = 44.6968\,;\, V_1 = \left(-0.9868,\, 0,\, -0.0631,\, -0.1490,\, 0\right) \\ &E_2 = 46.0224\,;\, V_2 = \left(-0.0022,\, 0,\, -1,\, 0.0068,\, 0\right) \\ &E_3 = 53.6070\,;\, V_3 = \left(-0.1494,\, 0,\, -0.0149,\, 0.9887,\, 0\right) \\ &E_4 = 53.3365\,;\, V_4 = \left(0,\, -0.0455,\, 0,\, 0,\, -0.999\right) \\ &E_5 = 48.2840\,;\, V_5 = \left(0,\, 0.999,\, 0,\, 0,\, -0.0455\right) \end{aligned} \tag{71}$$

where third and fourth set is associated to the WGM_x and WGM_y, since c_4 and c_5 are near one, respectively, which shows a difference of energy about $0.3meV$.

To evaluate the energy level of P_x in the arrangement of the electrons according to the Fig. 18a, we can consider three eigenbasis as:

$$P_x = c_1 s + c_2 p_y + c_3 p_x \tag{72}$$

which yields

$$\begin{aligned} &E_1 = 47.6672\,;\, V_1 = \left(-.9948,\, 0,\, 0.1019\right) \\ &E_2 = 54.8473\,;\, V_2 = \left(0.0775,\, 0,\, 0.997\right) \\ &E_3 = 49.3702\,;\, V_3 = \left(0,\, -1,\, 0\right) \end{aligned} \tag{73}$$

where second set with energy of $54.85\,meV$ is related to the P_x which is about $1.5\,meV$ higher than WGM_x and $1.3\,meV$ higher than WGM_y. This result is corresponding to the previously evaluated energy spectra in Fig. 19(a).

3.5 Magnetic Field Effect

Fig. 21 shows eigenergies of QD for $4.1\,meV$ s - p states splitting, where quantum numbers (n,l) related to the radial and azimuthal number are specified for each of the levels, while Table I shows the corresponding energies for each state.

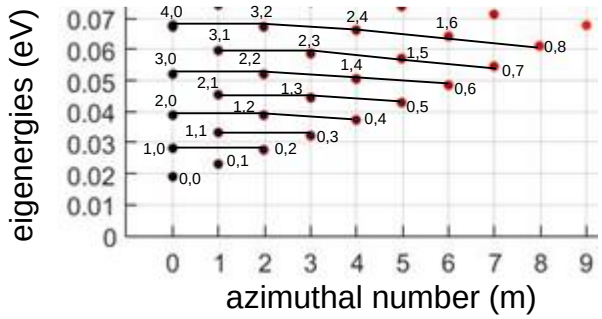

Figure 20 - Energy spectra for 4.1meV QD

Table 1 - Values corresponding to the Fig. 21

(0,0): 0.019	(0,3): 0.032	(1,3): 0.045	(0,6): 0.049	(4,0): 0.07
(0,1): 0.023	(2,0): 0.039	(0,5): 0.04	(3,1): 0.06	(3,2): 0.068
(1,0): 0.028	(1,2): 0.039	(3,0): 0.052	(2,3): 0.059	(2,4): 0.066
(0,2): 0.028	(0,4): 0.038	(2,2): 0.052	(1,5): 0.058	(1,6): 0.064
(1,1): 0.033	(2,1): 0.045	(1,4): 0.051	(0,7): 0.055	(0,8): 0.061

For 2D harmonic oscillator the energy levels can be determined from:

$$E_{n,l} = (2n + |l| + 1)\hbar\omega_0 \tag{74}$$

The energy levels of our system, near to the s & p states can be somehow equivalent to the 2D harmonic oscillator energy levels. To this end, we introduce a detuning parameter $\Delta_{n,l}$ as:

$$E_{n,l} = (2n + |l| + 1)(\hbar\omega_0 + \Delta_{n,l}) \tag{75}$$

The detuning parameter for each energy level is obtaind as following:

The energy levels of s - and p - states are considered to be $\hbar\omega_0$ and $2\hbar\omega_0$, respectively, with zero detuning parameters, where $\hbar\omega_0 = 4.1\,meV$ is s & p energy splitting:

$$E_{0,0} = \hbar\omega_0 \quad ; \quad \Delta_{0,0} = 0$$
$$E_{0,1} = 2\hbar\omega_0 \quad ; \quad \Delta_{0,1} = 0 \tag{76}$$

For a specific energy level like $E_{0,2}$, we can write the energy difference $E_{0,2}-E_{0,0}$ from Eqs. (75)-(76) as:

$$E_{0,2}-E_{0,0}=3(\hbar\omega_0+\Delta_{0,2})-\hbar\omega_0=8.537\text{meV} \tag{77}$$

Therefore, from Eq. (77), we can calculate:

$$\Delta_{0,2}=0.11meV \tag{78}$$

Similarly, for energy level $E_{0,3}$:

$$E_{0,3}-E_{0,0}=4(\hbar\omega_0+\Delta_{0,3})-\hbar\omega_0=13.31 \tag{79}$$

we can obtain:

$$\Delta_{0,3}=0.25meV \tag{80}$$

On the other hand, energy levels of 2D harmonic oscillator with applying magnetic field can be calculated from:

$$E_{n,l}=(2n+|l|+1)\sqrt{\frac{1}{4}(\hbar\omega_c)^2+(\hbar\omega_0)^2}-\frac{1}{2}l\hbar\omega_c \tag{81}$$

where ω_c is cyclotron frequency which can be evaluated from:

$$\hbar\omega_c=\hbar\frac{eB}{m^*}\quad;\quad m^*=0.08m_e \tag{82}$$

For instance for the magnetic field $B=1T$ we evaluate $\hbar\omega_c=1.4471meV$. For our case, we can insert $\Delta_{n,l}$ in eq. (81) as:

$$E_{n,l}=(2n+|l|+1)\sqrt{\frac{1}{4}(\hbar\omega_c)^2+(\hbar\omega_0+\Delta_{n,l})^2}-\frac{1}{2}l\hbar\omega_c \tag{83}$$

Therefore, for $E_{0,0}$ we can write:

$$E_{0,0}=\sqrt{\frac{1}{4}(\hbar\omega_c)^2+(\hbar\omega_0)^2}=\sqrt{\frac{1}{4}(1.4471)^2+(4.1)^2}=4.1634meV \tag{84}$$

while for zero magnetic field, $E_{0,0} = 4.1\,meV$ which shows that with magnetic field, energy level of s-state would be increased by $0.0634\,meV$.

For p-state, $l = -1$, we can write:

$$E_{0,1} = 2\sqrt{\frac{1}{4}(\hbar\omega_c)^2 + (\hbar\omega_0)^2} + \frac{1}{2}\hbar\omega_c = 2\sqrt{\frac{1}{4}(1.4471)^2 + (4.1)^2} + \frac{1}{2}1.4471 = 9.0503 \tag{85}$$

while for zero magnetic field, $E_{0,1} = 8.2$, which shows that, p-state would be increased by $0.8503\,meV$.

For wgm, $l = 2$ we can write:

$$E_{0,2} = 3\sqrt{\frac{1}{4}(\hbar\omega_c)^2 + (\hbar\omega_0 + \Delta_{0,2})^2} - \hbar\omega_c = 3\sqrt{\frac{1}{4}(1.4471)^2 + (4.1 + 0.11)^2} - 1.4471 = 11.3681 \tag{86}$$

while without magnetic field, $E_{0,2} = 12.63$, which shows that it would be decreased by $1.2619\,meV$

For wgm, $l = 3$,

$$E_{0,3} = 4\sqrt{\frac{1}{4}(\hbar\omega_c)^2 + (\hbar\omega_0 + \Delta_{0,3})^2} - \hbar\omega_c = 4\sqrt{\frac{1}{4}(1.4471)^2 + (4.1 + 0.25)^2} - \frac{3}{2}1.4471 = 15.5684 \tag{87}$$

For zero magnetic field $E_{0,3} = 17.4\,meV$ which shows that it is decreased by $1.8316\,meV$.

3.6 Experimental Result

Figure below shows experimental result for 4 meV QD. There are two close picks between s- and p-states which are related to the WGMs. Therefore, we can predict that these two close picks are corresponding to 2 electrons in WGM orbital, where each pick related to one of these 2 electrons. This result is corresponding to our numerically calculated energy spectra for 4 meV QD, Fig. 19 (a), in which 2 electrons are supposed to be in the excited state and 4 electrons in the ground state. In Fig. 19 (a), we similarly calculate the energy splitting between s- and p-states equal to 4 meV, and attain a WGM between these two states. Although, these two electrons have degenerate energy levels

in numerical result, but in experiment, this degeneracy can be split due to the defect in the dot. Besides, the size of the wavefunction distribution which is obtained by Near-Field Scanning Optical Microscopy (NSOM) is almost identical with single particle (numerical) calculation.

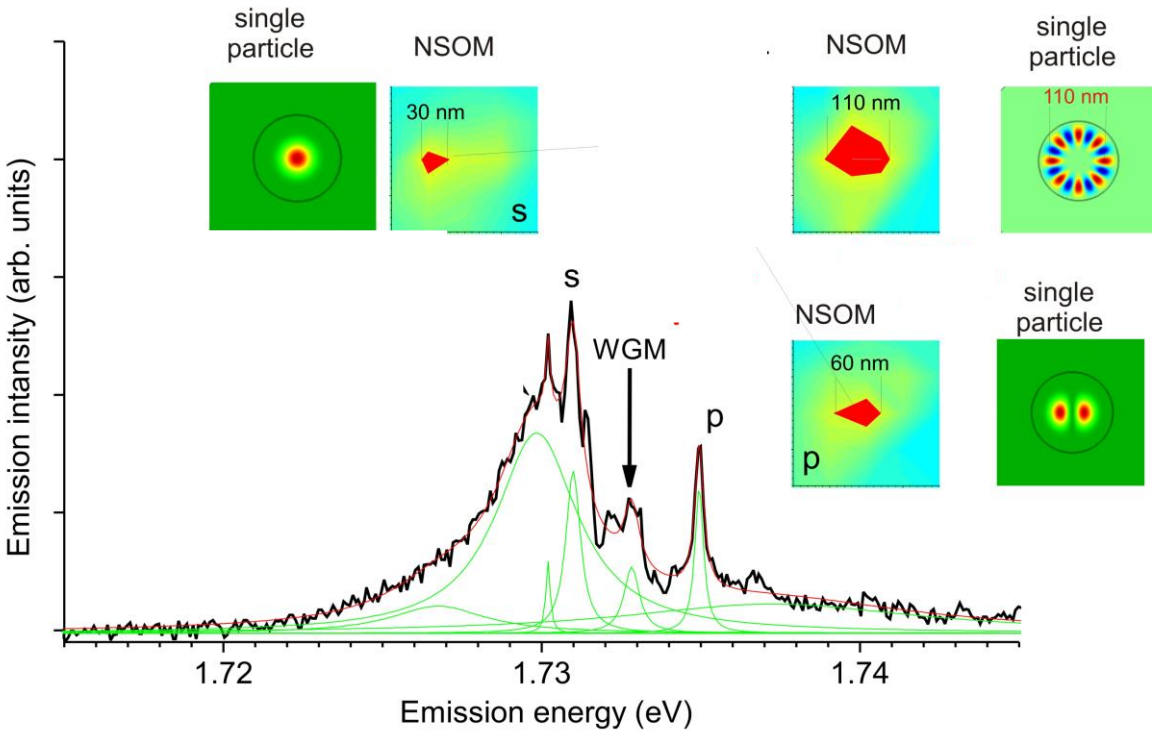

Figure 21 - Experiment result of energy spectra and wavefunction distribution for 4 meV QD

3.7 Surface Modes in Lateral QD

We could achieve surface states in lateral QD, in two orthogonal directions, φ- and z-directions.

3.7.1 WGMs

The resonance in the φ-direction which is referred to WGMs shows that WGM with higher angular momentum has larger effective length of the QD. Figure 22 shows WGMs with different angular momentums, in which the radius size of the resonance is increased for higher angular momentums.

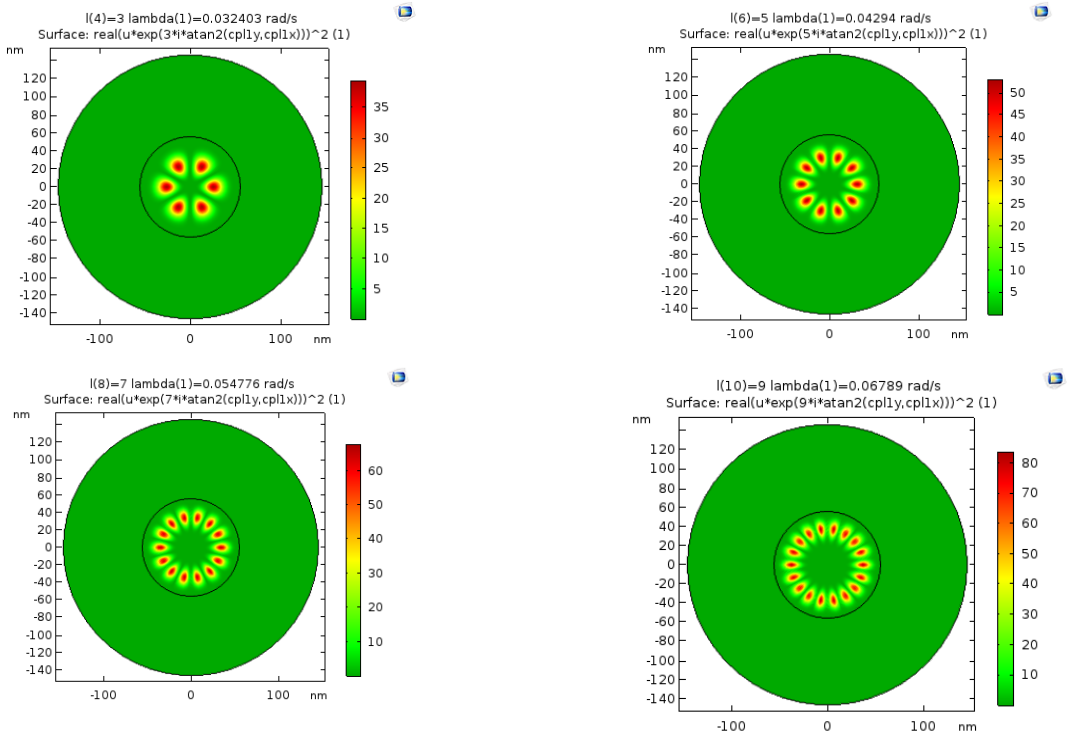

Figure 22 – WGMs from left to right, top: m=3, m=5, bottom: m=7, m=9.

3.7.2 Resonance across the Height

For each of the angular momentums (m), it is possible to achieve different modes of distribution along the height of the QD. Figure 23 shows these modes for m=7, which are related to 5th, 7th, 9th and 11th eigenvalues.

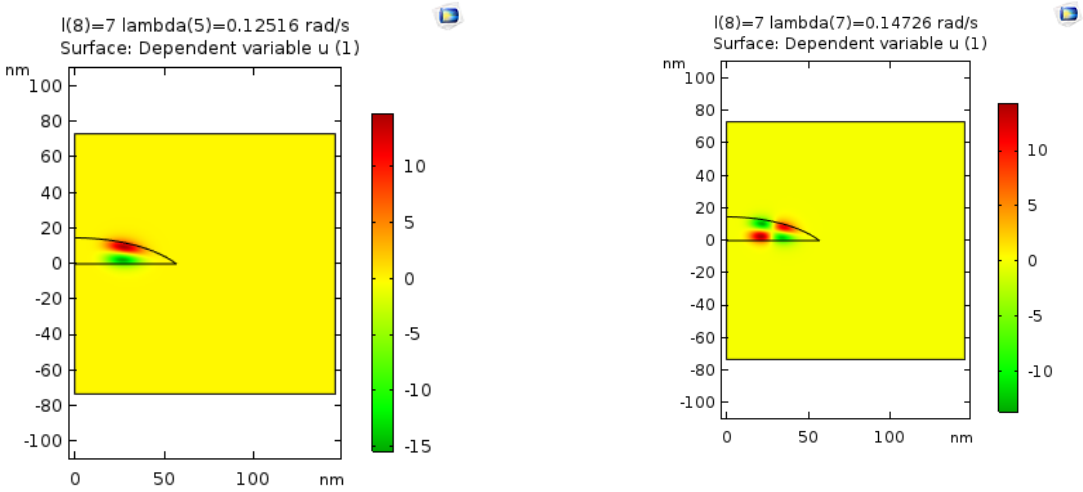

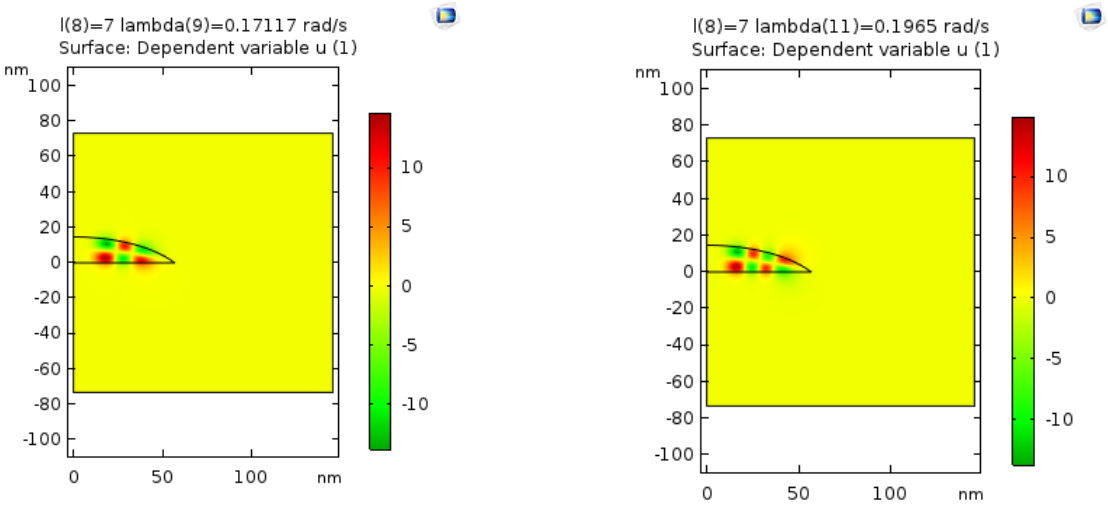

Figure 23 - Wavefunctions of QD for *m=7* ; from left to right, top: 5th, 7th, bottom: 9th, 11th eigenfunctions

For $6\,meV$ QD, for m=0, quantum number associated to the height, starts to change from 7th eigenvalue, while for 4 meV QD, it is 6th eigenvalue. Generally speaking, with increaing the s-p splitting, resonances across the height occur in a higher number of eigenstates. Figure 24 shows surface states of 10 *meV* QD which can exist only for m=0 (7th and 9th eigenvalues), m=1 (7th and 9th eigenvalues), m=2 (7th eigenvalue) and m=3 (7th eigenvalue). The interesting feature in this figure is that the confinement of the distribution in the QD is reduced which can be attributed to the both approaching the eigenvalues to the applied voltage, and also decreasing the height of QD.

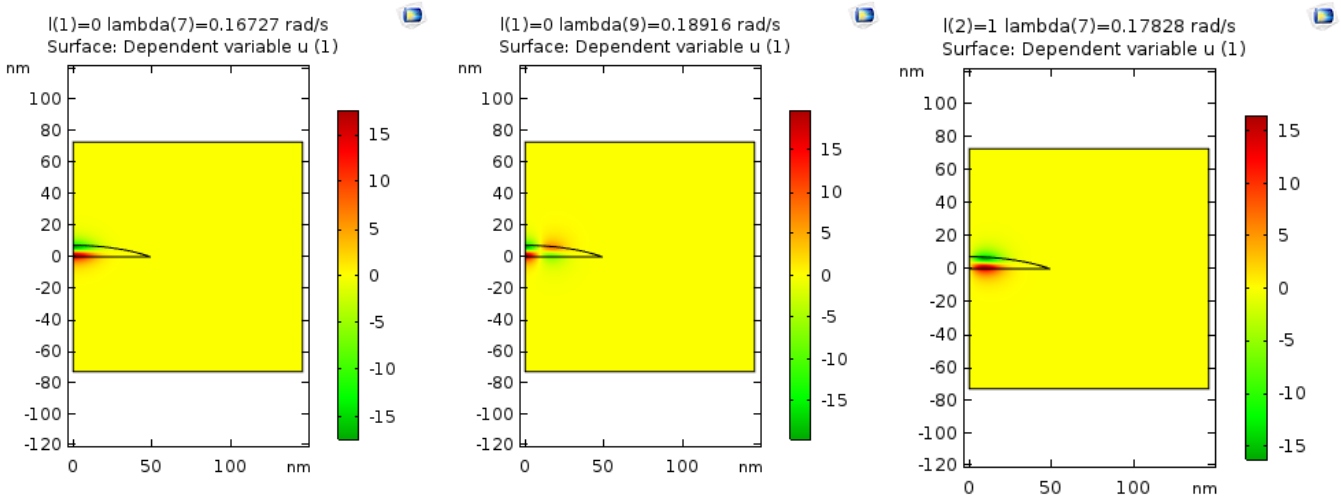

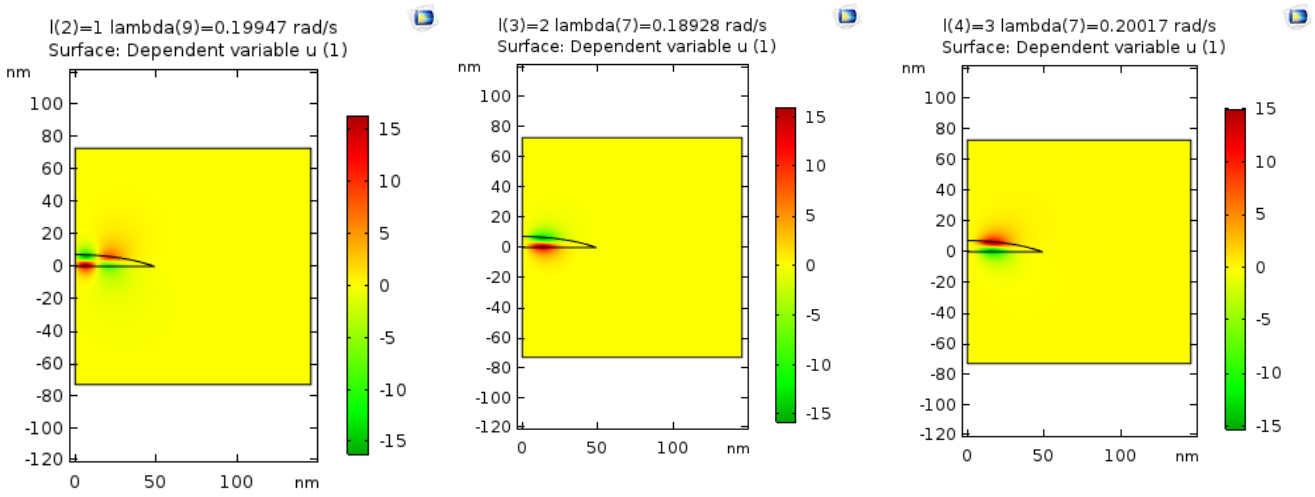

Figure 24 - Surface states of 6 meV QD; from left to right, top: 7th (m=0), 9th (m=0), 7th (m=1), bottom: 9th (m=1), 7th (m=2) , 7th (m=3) eigenfunctions

3.8 Perturbation

3.8.1 Lateral QD

Figure 25 shows that the perturbation which interfere a state can change it, otherwise it would be unaffected. This figure shows the comparison of three modes of surface states between unperturbed and perturbed QD, for 5th eigenvalue of m=0,1, 2 (unperturbed dot) and 6th eigenvalue of m=0, 5th eigenvalue of m=1,2 (perturbed dot).

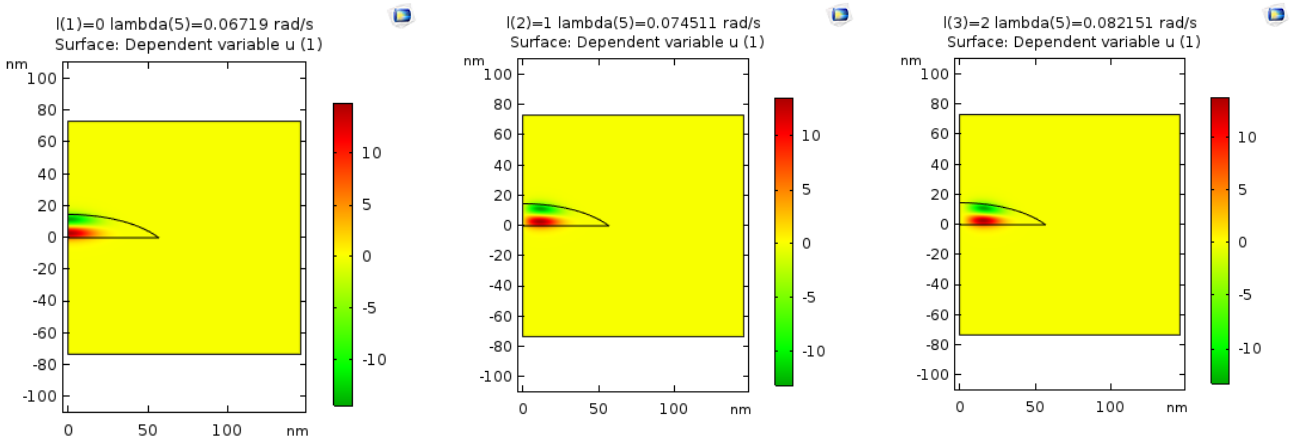

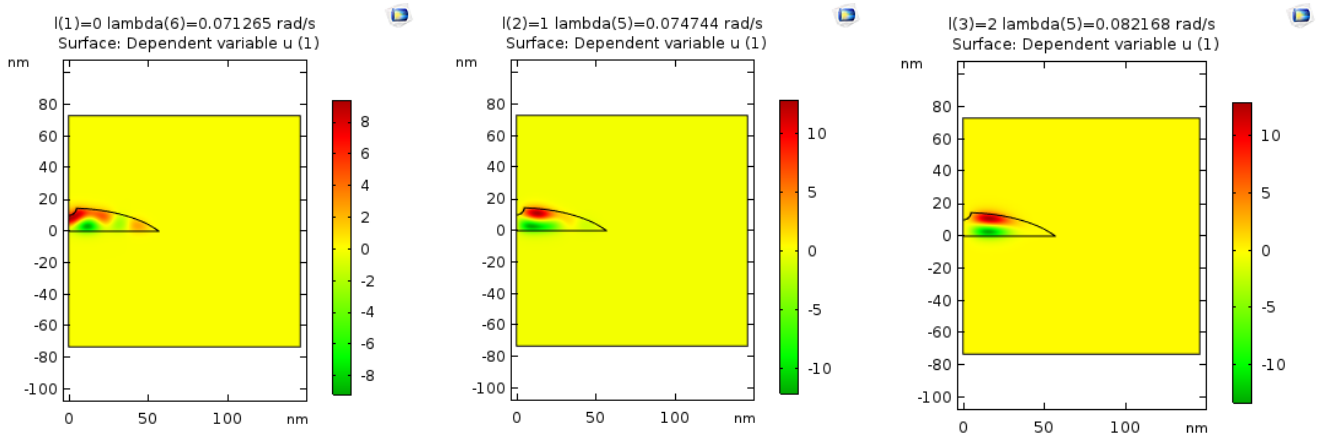

Figure 25 - Wavefunctions of 4 meV QD; from left to right, top (unperturbd): 5th (m=0), 5th (m=1), 5th (m=2), bottom (perturbed): 6th (m=0), 5th (m=1), 5th (m=2) eigenfunctions

It shows that the first mode which is mostly affected by perturbation is changed considerably, however, the other two modes are changed a little. The perturbation at the center of the dot leads the height of QD be decreased which cause the surface state for m=0 occur at a higher eigenvalue.

3.8.2 Spherical QD

Figure 26 shows that smooth deformation along the surface keep the surface states unchanged. This figure is related to the 1st, 2nd and 3rd eigenvalues of angular momentum m=10, for both spherical and deformed spherical dot, which shows that distribution and also the eigenvalues are almost identical in these dots. However, for higher order modes, due to the rapidly changing of the distribution along the surface, the deformation would change the states.

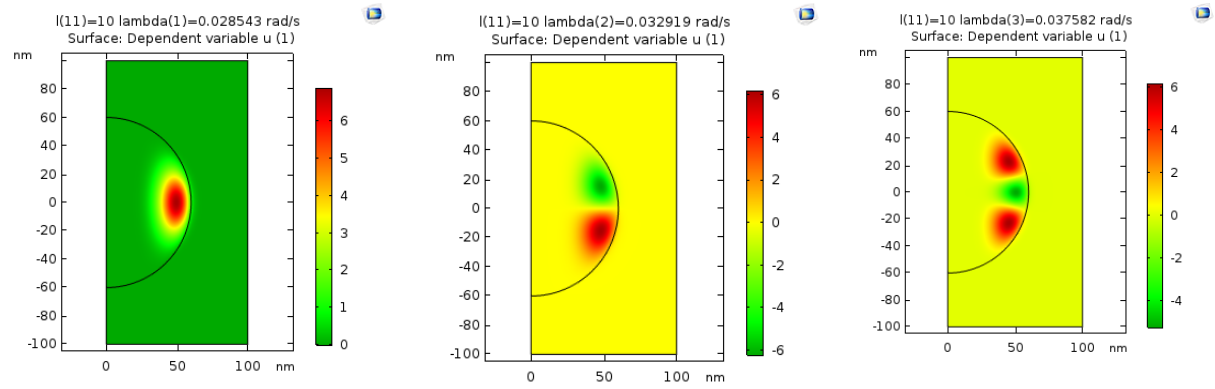

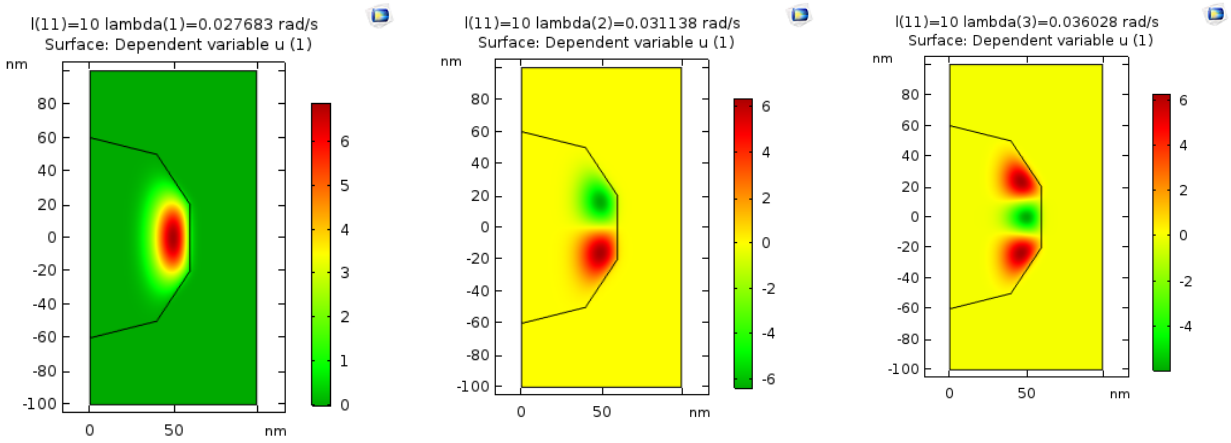

Figure 26 - Wavefunctions of spherical QD for first three eigenmodes of m=10, top: unperturbed, bottom: perturbed

3.8.3. Triangular QD

Figure 27 shows that by changing the geometry of the QD, we can handle the distribution of the electrons in the dot. This figure is related to the first three eigenmodes of angular momentum m=10 for the dots with the vertex at symmetrical and also unsymmetrical positions. It shows that electrons tend to concentrate at the vertex of these dot. Besides, in the unsymmetrical one, the distribution of electrons are more likely along the surface.

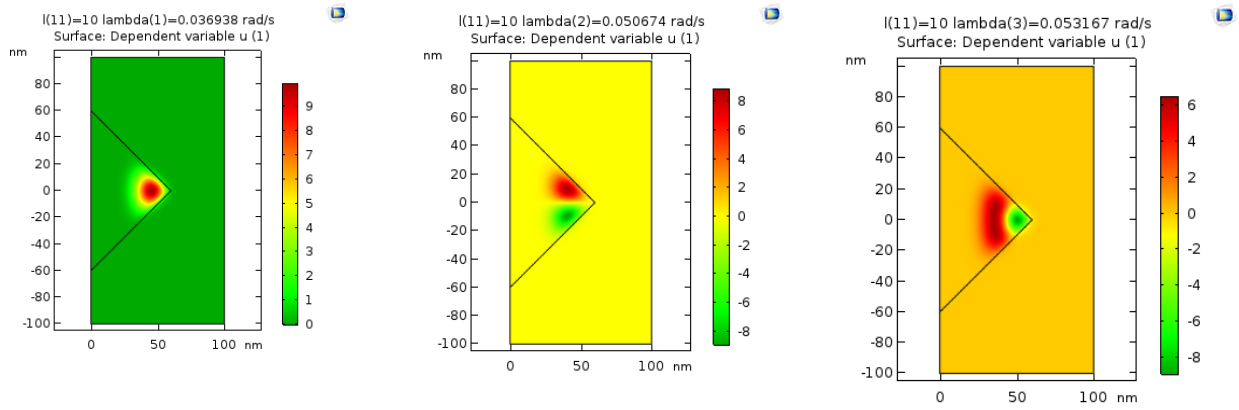

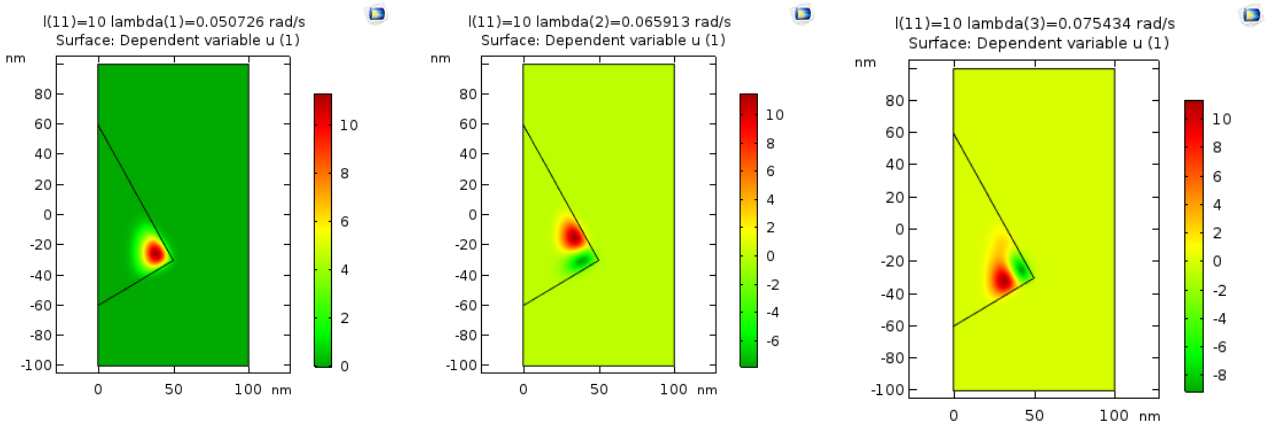

Figure 27 - Wavefunctions of triangular QD for first three eigenmodes of m=10, top: symmetrical vertex, bottom: unsymmetrical vertex

Conclusion

In this thesis, we study WGMs in Quantum Dots (QDs). In lateral QD the Coulomb interaction between the electrons plays a significant role in its energy spectra. We reveal that Coulomb interaction can be comparable to the interband transition energy, which cause some higher energy levels fall between the two lowest energy levels s- and p-states. Furthermore, some resonances along the height of QD are detected which are unusual in these dots. We reveal the perturbation and topological effect on the surface states in these dots as well as in spherical and triangular dots.

In these dots WGMs with higher angular momentums shows larger effective lengths in the QD. Resonances along the height of these dots show less confinement in the dot, with decreasing the height of the dot. It is shown that perturbation can affect the local distributions, while the non-local states would be unaffected. Smooth perturbation in spherical QD keep the surface states unaffected. Furthermore, surface states can be manipulated by changing the location of the vertex, in triangular dots.

References

[1] S. Tarucha, D. G. Austing, and T. Honda, "Shell Filling and Spin Effects in a Few Electron Quantum Dot" // Phys. Rev. Lett. ---1996 --- vol.77 --- no. 17

[2] S. Tarucha, D. G. Austing, Y. Tokura, W. G. van der Wiel, and L. P. Kouwenhoven, "Direct Coulomb and Exchange Interaction in Artificial Atoms" // Phys. Rev. Lett. --- Vol. 84 --- No. 2485.

[3] B. T. Miller, et al., "Few-electron ground states of charge-tunable self-assembled quantum dots" // Phys. Rev. B --- 1997-I ---vol. 56 --- no. 11.

[4] R. J. Warburton, et al.,"Coulomb interactions in small charge-tunable quantum dots: A simple model " // Phys. Rev. B ---1998-II --- vol. 58 --- no. 24.

[5] Yue Zhao, et al., "Creating and probing electron whispering-gallery modes in graphene" // Science --- 2015 --- vol. 348 --- no. 6235 --- pp. 672-675.

[6] G. Reecht, et al., "Oligothiophene Nanorings as Electron Resonators for Whispering Gallery Modes" // Phys. Rev. Lett. --- 2013 --- vol. 110 --- no. 056802.

[7] H. Xu, et al., "Superpersistent currents and whispering gallery modes in relativistic quantum chaotic systems" // Scientific Reports --- 2015 --- vol. 5 --- no. 8963.

[8] G. J. Ferreira and D. Loss, "Magnetically Defined Qubits on 3D Topological Insulators" // Phys. Rev. Lett. --- 2013 --- vol. 111 --- no. 106802.

[9] J Kapaldo, et al., "Ga–In intermixing, intrinsic doping, and Wigner localization in the emission spectra of self-organized InP/GaInP quantum dots " // J. Phys. D: Appl. Phys. --- 2016 --- vol. 49, no. 475301.

[10] A. M. Mintairov, J. L. Merz, J. Kapaldo, A. S. Vlasov, and S. A. Blundell, " Wigner Localization and Whispering Gallery Modes of Electrons in Quantum Dots " // Semiconductors --- 2018 --- vol. 52, no. 4, pp. 502–506.

[11] A. M. Mintairov, et al., "Control of Wigner localization and electron cavity effects in near-field emission spectra of In(Ga)P/GaInP quantum-dot structures " // Phys. Rev. B --- 2018 --- vol. 97, no. 195443.

[12] B. Brun, et al., "Wigner and Kondo physics in quantum point contacts revealed by scanning gate microscopy" // nature communication --- 2014 --- vol. 5 --- no. 4290.

[13] A. Iagallo, et al., "Scanning gate imaging of quantum point contacts and the origin of the 0.7 anomaly" // https://arxiv.org --- 2013.

[14] https://www.comsol.ru/model/conical-quantum-dot-723

[15] C. D. Sherill, "An Introduction to Hartree-Fock Molecular Orbital Theory" // http://vergil.chemistry.gatech.edu --- 2000.